MOLECULAR REPRODUCTION AND DEVELOPMENT 73:40–49 (2006)

# Overexpression of Ubiquitin Carboxyl-Terminal Hydrolase L1 Arrests Spermatogenesis in Transgenic Mice

YU-LAI WANG,[1] WANZHAO LIU,[1] YING-JIE SUN,[2] JUNGKEE KWON,[1,3] RIEKO SETSUIE,[1,4] HITOSHI OSAKA,[1] MAMI NODA,[4] SHUNSUKE AOKI,[1] YASUHIRO YOSHIKAWA,[3] AND KEIJI WADA[1]*

[1]*Department of Degenerative Neurological Diseases, National Institute of Neuroscience, NCNP, Kodaira, Tokyo, Japan*
[2]*Department of Anatomy and Structural Science, Yamagata University School of Medicine, Yamagata, Japan*
[3]*Department of Biomedical Science, Graduate School of Agricultural and Life Sciences, University of Tokyo, Bunkyo-ku, Tokyo, Japan*
[4]*Laboratory of Pathophysiology, Graduate School of Pharmaceutical Sciences, Kyushu University, Higashi-ku, Fukuoka, Japan*

**ABSTRACT** Ubiquitin carboxyl-terminal hydrolase 1 (UCH-L1) can be detected in mouse testicular germ cells, mainly spermatogonia and somatic Sertoli cells, but its physiological role is unknown. We show that transgenic (Tg) mice overexpressing *EF1α* promoter-driven UCH-L1 in the testis are sterile due to a block during spermatogenesis at an early stage (pachytene) of meiosis. Interestingly, almost all spermatogonia and Sertoli cells expressing excess UCH-L1, but little PCNA (proliferating cell nuclear antigen), showed no morphological signs of apoptosis or TUNEL-positive staining. Rather, germ cell apoptosis was mainly detected in primary spermatocytes having weak or negative UCH-L1 expression but strong PCNA expression. These data suggest that overexpression of UCH-L1 affects spermatogenesis during meiosis and, in particular, induces apoptosis in primary spermatocytes. In addition to results of caspases-3 upregulation and Bcl-2 downregulation, excess UCH-L1 influenced the distribution of PCNA, suggesting a specific role for UCH-L1 in the processes of mitotic proliferation and differentiation of spermatogonial stem cells during spermatogenesis. *Mol. Reprod. Dev. 73: 40–49, 2006.* © 2005 Wiley-Liss, Inc.

**Key Words:** UCH-L1; transgenic mouse; spermatogenesis; testis; apoptosis

## INTRODUCTION

Mammalian spermatogenesis is a complex process of cellular differentiation. Spermatogonia serve as the self-renewing stem cells for spermatogenesis and undergo mitotic divisions that yield primary spermatocytes (Matzuk and Lamb, 2002). In addition to germ cells, somatic Sertoli cells also are a major cell population in the testis, comprising the seminiferous tubule epithelium that nurtures germ cells (Imai et al., 2004).

Components of the ubiquitin system appear to be involved in different steps and processes during spermatogenesis (Baarends et al., 2000; Sutovsky, 2003). Ubiquitin is a highly evolutionarily conserved 76-residue polypeptide that plays a critical role in many cellular processes, including the cell cycle, cell proliferation, development, apoptosis, signal transduction, and membrane protein internalization (Williams et al., 2002). Ubiquitin appears to be expressed in mammalian testes/ovaries and embryos at all developmental steps, and its level is modulated by ubiquitynating and deubiquitynating enzymes. However, the details of the involvement of these enzymes in ubiquitin-dependent proteolysis during gametogenesis and fertilization remain uncertain. Several deubiquitynating enzymes were recently reported (Wilkinson, 2000; Wing, 2003) and have been classified as either ubiquitin carboxyl-terminal hydrolases (UCHs) or ubiquitin-specific processing proteases. UCHs liberate free ubiquitin by cleaving ubiquitin-containing covalent complexes, namely ubiquitylated small ribosomal proteins (L40, S27a) or tandemly conjugated polyubiquitin (e.g., UbB, UbC) (Wilkinson, 2000). UCHs can also hydrolyze bonds between ubiquitin and small adducts or unfolded polypeptides in vitro. Thus, UCHs are thought to serve dual functions: to salvage ubiquitin that has been trapped by reactions with low-molecular weight thiols/amines and to process polyubiquitin or ubiquitylated proteins.

In mice, there are at least four closely related low-molecular weight UCH family members, UCH-L1 and UCH-L3–5 (Kurihara et al., 2001; Osawa et al., 2001). The distribution and function of UCH-L4 and UCH-L5 are not clear. UCH-L3, however, is expressed ubiquitously, whereas UCH-L1 is selectively expressed in the testis/ovary and brain. Moreover, UCH-L1 is highly

Grant sponsor: Ministry of Health, Labour, and Welfare of Japan.

*Correspondence to: Dr. Keiji Wada, Department of Degenerative Neurological Diseases, National Institute of Neuroscience, NCNP, Kodaira, Tokyo 187-8502, Japan. E-mail: wada@ncnp.go.jp

Received 4 May 2005; Accepted 30 June 2005
Published online 21 September 2005 in Wiley InterScience (www.interscience.wiley.com).
DOI 10.1002/mrd.20364

expressed in mouse spermatogonia and somatic Sertoli cells but not in post meiotic germ cells (Kwon et al., 2004a). By contrast, UCH-L3 is detected mainly in spermatocytes and round spermatids (Kwon et al., 2004a). These two isozymes are considered to play important roles in the labeling/targeting of abnormal proteins for degradation via the ubiquitin-proteasome system (Wilkinson, 2000).

The gracile axonal dystrophy (*gad*) mouse is an autosomal recessive spontaneous mutant carrying an intragenic deletion of the gene encoding UCH-L1 (*Uchl1*). *gad* mice do not express UCH-L1 and thus are comparable to a *Uchl1* null mutant (Yamazaki et al., 1988; Saigoh et al., 1999). We recently showed that *gad* mice are resistant to the germ cell apoptosis during the first round of spermatogenesis (Kwon et al., 2005) and are also resistant to cryptorchid-induced testicular germ cell apoptosis (Kwon et al., 2004b). The expression of the apoptotic proteins p53, Bax, and caspases-3 was significantly lower in the immature testes, and the expression of both antiapoptotic and prosurvival proteins such as Bcl-2, Bcl-xL, XIAP, pCREB, and BDNF was significantly higher in *gad* mice following experimental cryptorchidism (Kwon et al., 2004b). These data prompted our hypothesis that UCH-L1 may be an important regulator of apoptosis during spermatogenesis. Experiments toward this end may provide additional evidence that UCH-L1 regulates spermatogenesis.

Our present report presents the characterization of the male sterility phenotype and the quantitation of apoptotic spermatocytes in *Uchl1* transgenic (Tg) mice. Constitutive expression of UCH-L1 in the testis results in a blockade of spermatogenesis at the pachytene stage of spermatocytes due to an increase in the number of apoptotic spermatocytes. These results indicate that excess UCH-L1 affects spermatogenesis during meiosis and, in particular, induces apoptosis in primary spermatocytes.

## MATERIALS AND METHODS

### Animals

We have previously described the Tg *Uchl1* mice carrying a 0.7-kb FLAG-tagged mouse *Uchl1* cDNA with the human translation elongation factor-1α (*EF-1α*) promoter (Osaka et al., 2003). Tg mice were identified by PCR analysis of tail DNA using specific primers (forward: ex6F, 5′-ATCCAGGCGGCCCATGACCTC-3′; reverse: ex9R, 5′-AGCTGCTTTGCAGAGAGCCA-3′). The *gad* mouse is an autosomal recessive mutant that was obtained by crossing CBA and RFM mice (Saigoh et al., 1999). All strains were maintained at our institute. To corroborate fertility disturbances in UCH-L1 Tg mice, a subset of the mice was continuously mated with wild-type C57BL/6J mice. The mating of two heterozygous Tg males with non-Tg females did not yield offspring until the age of 6 months despite grossly normal appearance. This was also the case for the mating of four heterozygous Tg females with non-Tg males. Their non-Tg littermates sired offspring normally. Finally, all six Tg mice were infertile, but they did not exhibit any apparent neurological phenotype during adulthood. Controls included nontransgenic (non-Tg) littermates and UCH-L1-deficient *gad* mice (Saigoh et al., 1999). Mice were sacrificed by cervical dislocation before tissue collection. Animal care and handling were in accordance with institutional regulations for animal care and were approved by the Animal Investigation Committee of the National Institute of Neuroscience, National Center of Neurology and Psychiatry of Japan.

### mRNA Isolation, and Exogenous *Uchl1* Expression Measured by Quantitative Real-Time RT-PCR

Total RNA from testes was isolated using the Trizol reagent (Gibco BRL Life Technologies, Bethesda, MD) and purified following the manufacturer's instructions. Real-time quantitative RT-PCR primer pairs flanking introns were used to specifically amplify transgene products, and their sequences were: forward, 5′-ATTT-CAGGTGTCGTGAGGAA-3′; and reverse, 5′-CCCAC-GTGGGAGACCTGATA-3′. Real-time quantitative PCR products, from 0.25–2.5 ng of reverse-transcribed cDNA samples, were detected using an ABI Prism, 7700 system (Applied Biosystems) as described previously (Aoki et al., 2002). β-Actin and GAPDH were used as endogenous controls. Results are expressed as the ratio of the mRNA level of the transgene to that of β-actin or GAPDH. As an external standard for quantitative analysis, the cDNA of the 3′-noncoding region of mouse *Uchl1* cDNA (covering the RT-PCR primers) was cloned and inserted into a pcDNA3 vector, purified, precisely quantified, and serially diluted 10-fold to 10 copies/μl. Standard curves were determined using linear regression analysis of the Ct values relative to plasmid copy numbers. In each real-time quantitative PCR assay, a 10-fold serially diluted cDNA template series was added to construct a standard curve for copy number. Each sample was analyzed in triplicate, and copy numbers were determined from each corresponding standard curve by the ratio of Tg *UCH-L1* to mouse *Uchl1*.

### Histological Observations, Immunohistochemistry, and Immunofluorescence

Morphological studies were performed on six male controls and two male Tg mice (Tg21 and Tg22, both 6 months old). The two control groups consisted of three non-Tg wild-type C57BL/6J mice, 6 months old, littermates, and three *gad* mice, age 4 months. Testes were fixed in 4% paraformaldehyde for 24 hr and embedded in paraffin. Serial 5-μm sections were used for histology after hematoxylin–eosin staining as well as for immunohistochemistry and the TUNEL assay. Primary monoclonal or polyclonal antibodies against the following proteins were used at the final dilutions indicated: UCH-L1 (RA95101, Ultraclone, Lucigen, Middleton, WI, 1:2,000), FLAG (FM2, Sigma, St. Louis, MO, 1:500), PCNA (PC10, Santa Cruz Biotechnology, Santa Cruz, CA, 1:200), PCNA (Clone 24, BD Transduction

Laboratory, Lexington, KY, 1:2,000), vimentin (Zymed, 1:100), and ubiquitin (Dako, Carpenteria, CA, 1:400). For controls, the primary antibody was replaced with normal rabbit serum or was omitted (these controls always yielded negative staining). For immunofluorescence studies, secondary antibodies were anti-mouse-Cy3 or -FITC or anti-rabbit-conjugated-Cy3 or -FITC (Jackson ImmunoResearch, West Grove, PA, 1:500).

### TUNEL Assay

TUNEL staining was performed according to the original protocol, with modifications (Harada et al., 2004). The number of apoptotic cells was determined by counting positively stained nuclei in 30 tubule cross-sections per testis section in each testis (Kwon et al., 2004b). For clarity and brevity, we also counted all the TUNEL-stained cells within the entire cell population of testicular tubules in each section. In addition, we also counted the apoptosis-positive tubules (i.e., tubules containing at least one apoptotic cell) in each testis.

### Western Blotting

Protein lysates were prepared from mouse testes as described (Kwon et al., 2004b). Approximately 20 μg of total protein was loaded per lane on 15% SDS–PAGE gels. Primary antibodies (diluted as indicated) were used to detect the following proteins: UCH-L1 (RA95101, 1:5,000), FLAG (FM2, Sigma, 1:2,000), Bcl-2 (Cell Signaling, Beverly, MA, 1:1,000), caspase-3 (Cell Signaling, 1:400), polyubiquitin (FK2 clone, Medical & Biological Laboratory, Nagoya, Japan, 1:1,000), and monoubiquitin (U5379, Sigma, 1:1,000). Blots were further incubated with peroxidase-conjugated goat anti-mouse IgG or goat anti-rabbit IgG (1:5,000; Pierce, Rockford, IL) for 1 hr at room temperature. Immunoreactions were visualized using the SuperSignal West Dura extended duration substrate (Pierce) and analyzed with a ChemiImager (Alpha Innotech, San Leandro, CA). ChemiImager data were analyzed using AlphaEase software (Alpha Innotech) to yield the relative level of each protein.

## RESULTS

### Sterile Phenotype of *Uchl1* Tg Mice

We initially attempted to overexpress *Uchl1* in neurons using a Tg construct containing the *EF-1α* promoter (Mizushima and Nagata, 1990). The transgene was also strongly expressed in gonads as well as other Tg mice via the same promoter (Furuchi et al., 1996). We obtained six Tg mice having high transgene copy number, each of which most likely carried the transgene in a unique genomic location (see below). Four of these mice were females (Tg11, Tg12, Tg43, Tg81) and two were males (Tg21 and Tg22). Unexpectedly, all of these Tgs were sterile. Thus, it was not possible to maintain Tg lines during the course of these experiments. However, in addition to the sterile phenotype, the six independent Tg mice showed a similar pattern of *Uchl1* transgene expression and common pathological defects, the latter being limited to the testes or ovaries. The Tg loci were generated by random integration rather than by site-specific recombination, and thus the animals produced by our Tg procedure usually had more than one transgene integrated at each chromosomal site (Kroll and Amaya, 1996). Therefore, in each of the six Tg mice, the transgene most likely integrated into a different genomic site, raising the possibility of different position-dependent effects. Our data showed that we obtained multiple animals with similar patterns or levels of *Uchl1* transgene expression and with common pathological defects, suggesting the phenotypes reflect position-independent expression (i.e., independent of the position of transgene insertion). Thus, these Tg mice had similar infertile phenotypes that may be attributed to the overproduction of UCH-L1. Numerous gene inactivation studies have identified gene products involved in male fertility, but in most cases female reproduction was unaffected or weak damaged (Yuan et al., 2000). However, both male and female *Uchl1* Tg mice were infertile, although there were clear differences in germinal cell maturation, suggesting that UCH-L1 is required for both spermatogenesis and oogenesis. Therefore, six independent Tg founders, notably two males (Tg21 and Tg22), were analyzed in our present study.

The mating of two heterozygous Tg males with non-Tg females did not yield offspring until the age of 6 months, despite grossly normal appearance. This was also the case for the mating of four heterozygous Tg females with non-Tg males. Their non-Tg littermates sired offspring normally. At autopsy, the testes of both Tg21 and Tg22 appeared grossly smaller than those of non-Tg mice. The testes weight of Tg21 (77 mg) and Tg22 (70 mg) was only 42% and 38%, respectively, relative to non-Tg males ($183 \pm 16$ mg), demonstrating that mice overexpressing UCH-L1 display profoundly defective testis development.

### Expression Levels of the *Uchl1* Transgene

We used RT-PCR and primers specific for the *Uchl1* transgene to compare transgene expression levels in the testes or ovaries of the six Tg mice. There was some variation between animals (Fig. 1A). All the Tgs expressed a similar level of endogenous *Uchl1* mRNA (Fig. 1A); quantitation of absolute Tg *Uchl1* copy numbers using real-time quantitative RT-PCR showed that all six Tgs expressed 2.9–6.8-fold more *Uchl1* transgene mRNA compared with endogenous mRNA (4.5, 3.6, 6.2, 3.7, 2.9, and 6.8 for Tg21, Tg22, Tg11, Tg12, Tg43, and Tg81, respectively). Relative UCH-L1 protein expression was similar among four of the Tgs ($76.1 \pm 5.2$; Fig. 1B) but was somewhat higher in Tg 21 (100) and Tg81 (106.2). The average level of endogenous UCH-L1 expression in Tg mice was ~91% relative to non-Tg mice (Fig. 1B).

Immunohistochemistry of testicular sections using an antibody against FLAG revealed that exogenous UCH-L1 localized mainly in spermatogonia and Sertoli cells (Fig. 2E), similar to the localization of endogenous UCH-L1 (Fig. 2A). Endogenous UCH-L1 localized to both the cytoplasm and nucleus of spermatogonia and Sertoli

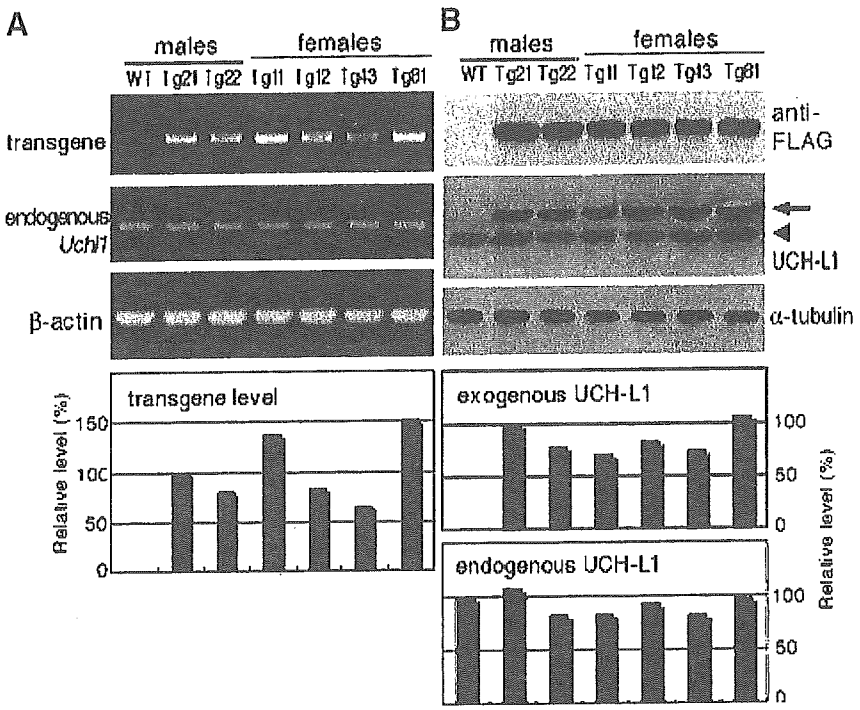


**Fig. 1.** Expression of transgenic ubiquitin carboxyl-terminal hydrolase 1 (UCH-L1) in the testes of Tg21 and Tg22 male mice. **A**: Transgenic *Uchl1* mRNA levels in the testes. RT-PCR showed high levels of *Uchl1* transgene mRNA in both Tg21 and Tg22 as well as in all ovaries from four female Tg mice. All Tg mice had a normal level of endogenous *Uchl1* mRNA. The relative expression level is indicated below each lane (as a percentage, scaled to β-actin in each lane). **B**: Western blot analysis of testicular or ovarian lysates. Both endogenous and exogenous UCH-L1 were detected with anti-UCH-L1, whereas exogenous UCH-L1 was specifically detected by anti-FLAG. Exogenous UCH-L1 (arrow) is slightly larger than endogenous UCH-L1 (arrowhead). WT, non-Tg wild-type.

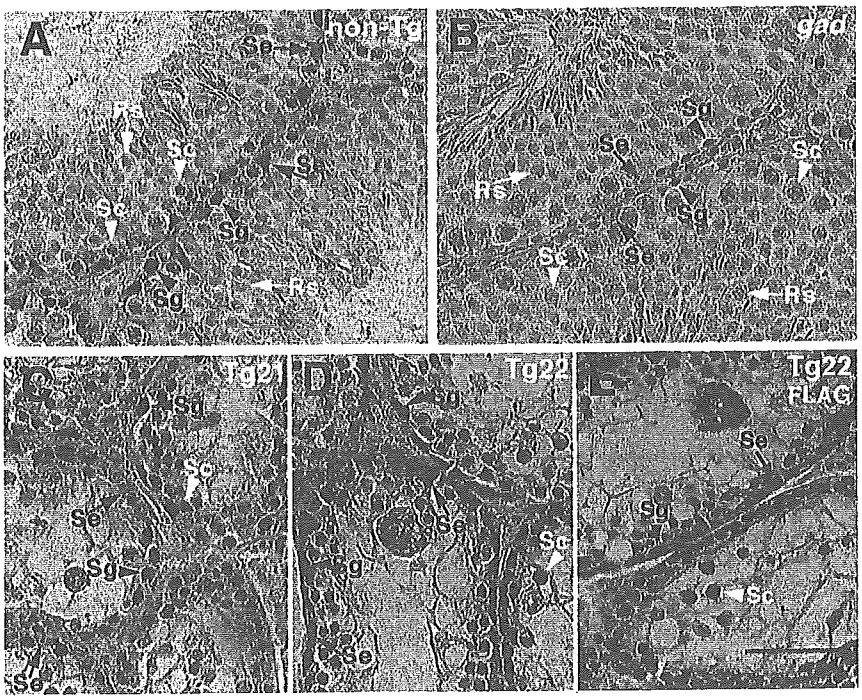


**Fig. 2.** Immunostaining of FLAG and UCH-L1 in *Uchl1* Tg mice shows high levels of UCH-L1 in testicular tubules. UCH-L1 immunostaining is clearly present in spermatogonia (Sg) and Sertoli cells (Se) of a non-Tg mouse (**A**) but not in a *gad* mouse (**B**). In contrast, in the testes of two Tg males, the most intense UCH-L1 immunoreactivity occurs predominantly in spermatogonia (Sg, arrowheads) and Sertoli cells (Se, arrows) but not in the primary spermatocytes (Sc, white arrowheads; **C**, Tg21; **D**, Tg22). **E**: Immunostaining of FLAG confirmed the transgene-derived UCH-L1 proteins in spermatogonia (Sg, arrowheads) and Sertoli cells (Se, arrows) but not in the primary spermatocytes (Sc, white arrowheads; Tg22). Magnification: ×400. Scale bar, 50 μm.

cells in the testes of non-Tg males; however, localization was not apparent around pachytene spermatocytes or round, elongated spermatids (Fig. 2A). This distribution of UCH-L1 is in good agreement with previous reports (Kon et al., 1999; Kwon et al., 2004a). Compared with non-Tg males, overexpression of UCH-L1 in seminiferous tubules of Tg males (Tg21 and Tg22) occurred predominantly in spermatogonia and Sertoli cells, and was weakly positive or negative in spermatocytes (Fig. 2C,D). These data coincided with strong induction of the *Uchl1* transgene. Tg mice expressed a higher level of total UCH-L1 (both endogenous and exogenous), suggesting a correlation between excess UCH-L1 and sterility.

### Morphological Examination

Histopathological analysis of testes from 6-month-old Tg21 and Tg22 revealed terminal loss of differentiated germ cells and a large number of pachytene spermatocytes that had degenerated (with condensed nuclei and giant cells) and been sloughed off, forcing an altered structure of the seminiferous tubules such that they appeared almost empty (Fig. 3A). The deformed seminiferous tubules also contained numerous arrested spermatocytes (Fig. 3A, arrowheads) and multinucleated giant cells (arrows). In contrast, the seminiferous tubules of *gad* mice were nearly intact, as in non-Tg males (data not shown). In non-Tg males, seminiferous tubules containing elongated spermatids in the inner layer were readily detected (data not shown), whereas these tubules were scarcely detectable in Tg21 (Fig. 3A) and Tg22. On the other hand, the four female Tg mice displayed a variety of phenotypes, including an increased number of apoptotic oocytes and granulosa cells relative to non-Tg females, leading to infertility (data not shown).

In non-Tg (Fig. 3B) and *gad* mice (Fig. 3C), only a few TUNEL-positive cells were identified, located at the periphery of the tubule. However, many fewer TUNEL-positive cells were detected in the Tg males (Fig. 3D,E), and cell morphology indicated that most of these positive cells were primary spermatocytes. However, neither the TUNEL assay nor microscopy revealed evidence of apoptosis in spermatogonia or Sertoli cells. We quantitatively assessed germ cell apoptosis in Tg, non-Tg, and *gad* mice by calculating the number of apoptotic cells per tubules in each testis. This value was 25 times higher in Tg testes compared with non-Tg or *gad* testes (the averages ± SD were as follows: $553 \pm 72$, $n = 2$ in Tg testes; $22 \pm 4.2$, $n = 3$ in non-Tg; and $21 \pm 5.3$, $n = 3$ in *gad*). The percentage of apoptosis-positive tubules in Tg testes was also significantly higher than in non-Tg or *gad* mice (the averages ± SD were as follows: $95.3 \pm 2.7$, $n = 2$ in Tg testes; $7.4 \pm 2.2$, $n = 3$ in non-Tg; and $7.1 \pm 1.8$, $n = 3$ in *gad*).

A control section of caput epididymis, an androgen-dependent organ, from same Tg mice was investigated. No UCH-L1 overexpressing was detected, and no pathological symptoms could be observed in the epididymis (data not shown).

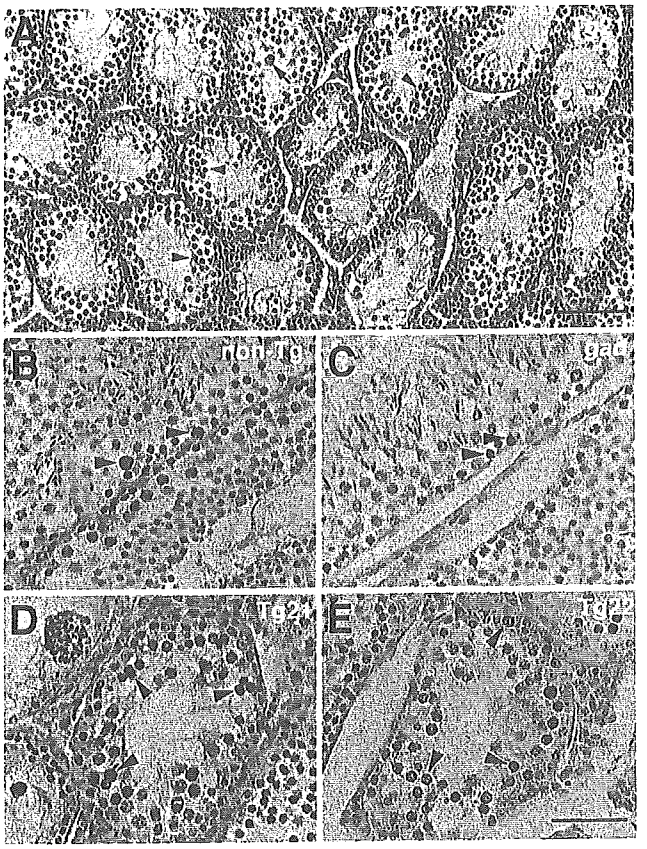


**Fig. 3.** Histopathology and TUNEL assay in situ. **A**: Hematoxylin–eosin staining of testis sections from the Tg21 male mouse shows defective spermatogenesis. Arrowheads indicate arrested spermatocytes and arrows indicate giant cells. Round spermatocytes and spermatids were rarely observed. **B–E**: Examples of TUNEL-positive cells characterized by the robust deposition of the reddish brown reaction product in sections of testis from non-Tg (B), *gad* (C), and Tg mice (D, Tg21; E, Tg22). Sections were counterstained with hematoxylin. A large number of TUNEL-positive cells were clearly observed at the periphery of the seminiferous tubule (arrowheads) in Tg21 (D) and Tg22 (E), whereas a lesser number of positives were apparent in non-Tg (B) or *gad* mice (C). Most of these positive cells appeared to be primary spermatocytes. Magnification: (A) ×100; (B–E) ×400. Scale bar in (A) 200 μm; (E) 50 μm.

### UCH-L1 Relates to the Expression of PCNA

PCNA expression is associated with cell proliferation and DNA synthesis during S phase of the cell cycle and DNA repair in non-dividing cells (Kelman, 1997; Toschi and Bravo, 1988). Unlike UCH-L1, which is abundant in brain, PCNA is not detectable in the central nervous system (Saigoh et al., 1999; Williams et al., 2002). In the testis, PCNA is expressed in germ cells and Sertoli cells, and the nuclear localization of PCNA overlaps with that of UCH-L1 in monkey testis (Tokunaga et al., 1999). Our recent study showed that mice lacking UCH-L1 have significantly decreased numbers of PCNA-positive cells in seminiferous tubules (Kwon et al., 2003). These results led us to hypothesize that UCH-L1 may be closely associated with spermatogonial proliferation activity, possibly to maintain the primordial nature of these cells. We thus immunostained testes for PCNA

and UCH-L1. In non-Tg and *gad* testes, PCNA-positive staining was confined to spermatogonia and primary spermatocytes and was not evident in Sertoli cells (Fig. 4A,D,B,E) Similarly, the percentage of PCNA-positive spermatogonia and spermatocytes in the seminiferous tubules of *gad* mice was significantly lower than that of non-Tg mice (Fig. 4A,D,B,E) as we previously observed (Kwon et al., 2003). In contrast, Tg mouse testes showed greater PCNA staining in these cells; surprisingly however, staining was observed in nearly all arrested primary spermatocytes but not in spermatogonia (Fig. 4F). These findings suggest that UCH-L1 plays a specific role in mitotic proliferation. To further clarify the effect of UCH-L1 on PCNA levels, FLAG-tagged *Uchl1* was transfected into GC-1, a germ cell line derived from type B spermatogonia (Hofmann et al., 1992). UCH-L1 (anti-FLAG, Fig. 4G,I, green) and PCNA (Fig. 4H,I, red) were then visualized using immunofluorescence microscopy. Cells transfected with *Uchl1* showed lower PCNA immunoreactivity compared with mock-transfected cells (Fig. 4G), consistent with the assertion that PCNA is downregulated by UCH-L1 in vivo. However, no change of PCNA level was observed in *Uchl3* transfected cells (data not shown),

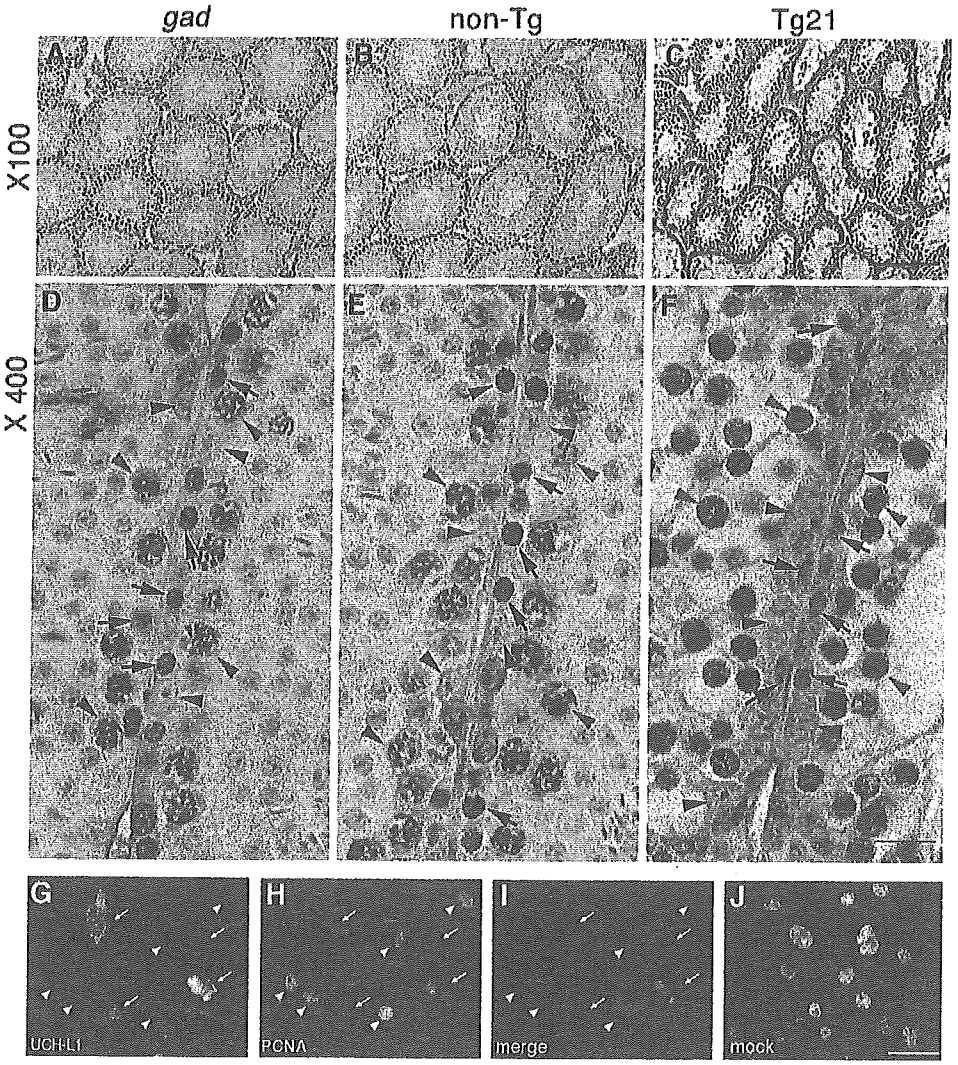


**Fig. 4.** PCNA immunostaining in the testes of a *gad* mouse (**A, D**), a non-Tg mouse (**B, E**), a Tg mouse (**C, F**; Tg21), and in the transient transfection assay with UCH-L1 using GC-1 cells (**G–J**). In *gad* and non-Tg testes, positive immunostaining was confined to spermatogonia (D, E; black arrows) and primary spermatocytes (D, E; red arrowheads), and staining was not seen in Sertoli cells (D, E; black arrowheads). In contrast, cell staining was more intense in the testis of Tg mice; however, this intensity was observed in almost all arrested primary spermatocytes (F; red arrowheads) but not in spermatogonia (F; black arrows). The staining of non-Tg and *gad* mice was essentially identical. However, nearly all the primary spermatocytes from Tg mice had relatively strong reactivity compared with spermatogonia that had very faint PCNA reactivity (black arrows). Plasmid pCIneo-*Uchl1* (G–I) or vector alone (J, mock) was transfected into GC-1 cells and expressed. Antibodies against FLAG (Sigma, monoclonal) and PCNA (BD Transduction Laboratory, polyclonal) were used to detect exogenously expressed UCH-L1 (G, I, green) and endogenous PCNA (H, J, I, red), respectively. Cells expressing a high level of UCH-L1 (G, white arrows) had a relative low level of PCNA (H, white arrows), whereas cells expressing a low level of UCH-L1 (H, white arrowheads) had high PCNA levels (H, white arrowheads). Magnification: (A–C) ×100; (D–J) ×400. Scale bar: **Upper panels** (see **panel C**), 200 μm; **middle panels** (see **panel F**), 50 μm; **lower panels** (see **panel J**), 50 μm.

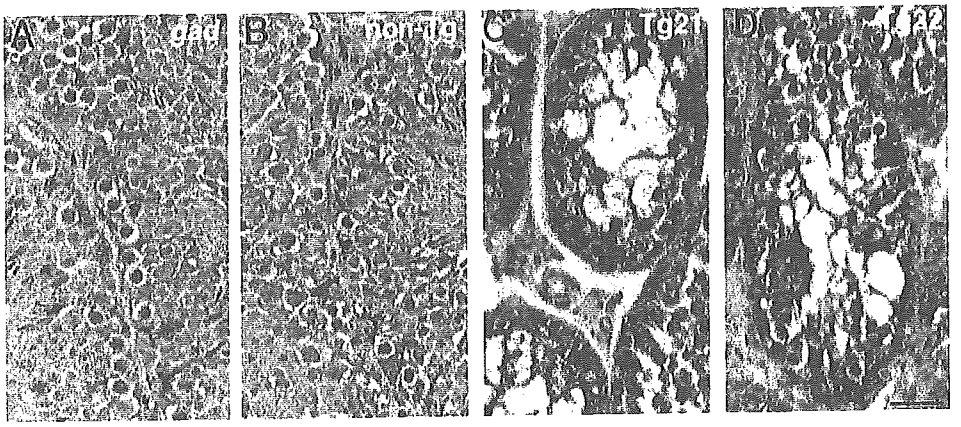


**Fig. 5.** Vimentin immunostaining in the testes of a *gad* mouse (**A**), a non-Tg mouse (**B**), and Tg mice (**C**, Tg21; **D**, Tg22). No difference was observed in the pattern and density of vimentin staining in Sertoli cells between *gad* (A) and non-Tg testes (B). In contrast, Sertoli cell staining was more intense in the Tg mice (C, D). Magnification: ×400. Scale bar, 200 μm.

suggesting the specificity of UCH-L1 effect on PCNA levels.

### Sertoli Cells Exhibit High-Level Vimentin Expression in Tg Mice

We examined the immunoreactivity to vimentin, which is a marker of Sertoli cells (Oke and Suarez-Quian, 1993; Mori et al., 1997). Vimentin immunostaining was observed in Sertoli cells, and there is no difference between *gad* and non-Tg mice (Fig. 5A,B). In contrast, very strong expression of vimentin was observed in almost all Sertoli cells throughout the cytoplasm in Tg mice (Fig. 5C,D).

### Bcl-2 Downregulation and Caspase-3 Upregulation in Tg Mice

The two key proteins, Bcl-2 and caspases-3 that involved in testicular germ cell apoptosis are especially altered during spermatogenesis or stress-induced germ cell apoptosis in *gad*mice (Harada et al., 2004; Kwon et al., 2004b, 2005). We thus examined the expression of these proteins in Tg and non-Tg testes to determine whether they are actually involved in countering increased apoptosis. Bcl-2 expression was downregulated in the testes of Tg mice compared with non-Tg mice (Fig. 6). In contrast to non-Tg mice, Tg mice had an elevated level of the activated caspase-3 subunit, p17 (Fig. 6), controversial to that observed in the retina of *gad* mice after ischemic injury (Harada et al., 2004). These results are consistent with the profound difference in UCH-L1 expression in these two mouse lines.

### Upregulations of both Mono- and Poly-Ubiquitin in Tg Mice

Our recent studies suggested novel functions for UCH-L1, namely that it effectively upregulates ubiquitin levels at the post-transcriptional level (Osaka et al., 2003) and that ubiquitin induction plays a critical role in regulating cell death during cryptorchid injury–mediated germ cell apoptosis (Kwon et al., 2004b). Moreover, the testes of mice expressing K48R mutant ubiquitin are protected from cryptorchid injury (Rasoulpour et al., 2003). Given this information, we examined ubiquitin levels in *Uchl1* Tg mice. As expected, ubiquitin expression was strong in testicular cells of Tg mice (Fig. 7C,D), particularly in the arrested spermatocytes, but its expression was low in *gad* mice (Fig. 7B) compared with non-Tg mice (Fig. 7A). These data provide additional evidence that ubiquitin expression is induced upon UCH-L1 overexpression. To determine whether the increased ubiquitin staining represented monoubiquitin or polyubiquitin, we next examined the levels of both ubiquitin forms via immunoblotting (Fig. 7E). As expected, mono- and poly-ubiquitin levels in Tg mice were substantially higher than in non-Tg mice. A *gad* mouse control had relatively low levels

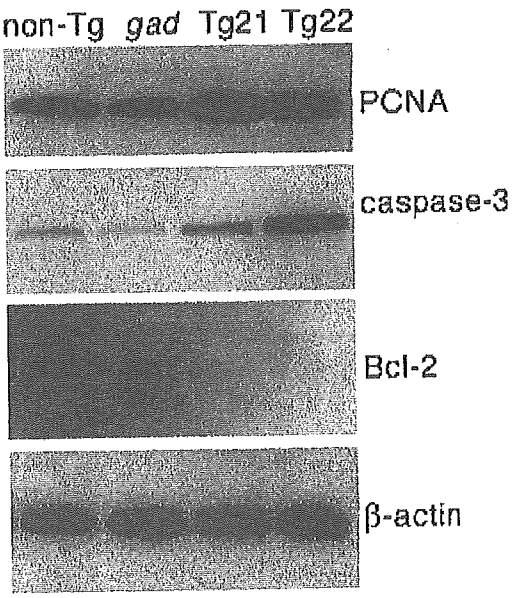


**Fig. 6.** Western blot analysis of Tg mouse testicular lysates. Consistent with the immunohistochemistry results, PCNA and caspase-3 substantially accumulated in Tg mice. However, the expression of antiapoptotic Bcl-2 decreased compared with non-Tg or *gad* mice.

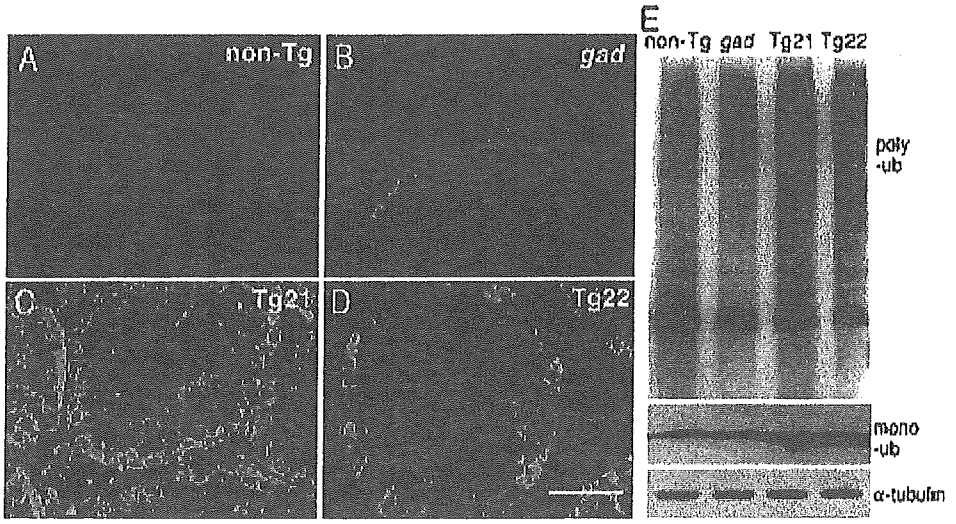


**Fig. 7.** The levels of mono- and poly-ubiquitin in the testes of non-Tg and Tg males. Double immunostaining for UCH-L1 and ubiquitin in the testis (**A**, non-Tg; **B**, *gad*; **C**, Tg21; **D**, Tg22). All strongly UCH-L1-positive cells (green) were also strongly positive for ubiquitin (red) in the two male Tg mice. Scale bar, 50 μm. **E**. An immunoblot showing that both mono- and poly-ubiquitin expression were significantly increased in the two Tg mice compared with non-Tg and *gad* mice (ub, ubiquitin).

of both mono- and poly-ubiquitin (Fig. 7E). These findings are consistent with previous studies and support the hypothesis that UCH-L1-mediated spermatocyte apoptosis involves the induction of ubiquitin expression.

## DISCUSSION

Apoptosis in testicular germ cells is regulated by a complicated signal transduction pathway; however, the molecular mechanisms regulating this process are uncertain. We recently showed that *gad* mice, lacking UCH-L1 function, are resistant to apoptotic stress (Harada et al., 2004; Kwon et al., 2004b). These observations conclusively indicate that UCH-L1 plays a role in germ cell death during experimental stress-induced apoptosis. We thus hypothesized that germ cell apoptosis is directly induced by excess UCH-L1. To test this hypothesis, we utilized three mouse lines, wild-type (non-Tg), *gad* and *Uchl1* Tgs, which differ with respect to UCH-L1 expression. In Tg mice, germ cell apoptosis was barely detectable in spermatogonia or Sertoli cells, both of which strongly expressed UCH-L1. Apoptosis was observed mainly in primary spermatocytes, which had weak or negative UCH-L1 expression although they are derived from spermatogonia. These data suggest that excess UCH-L1 in fact does not directly induce apoptosis in spermatogonia or somatic Sertoli cells. These data further provoke the question of why apoptosis occurs during spermatocyte meiosis.

In our *Uchl1* Tg mice, there was no evidence of spermatogonia or Sertoli cell apoptosis despite the fact that these cells had stronger UCH-L1 expression compared with non-Tg mice. Accordingly, it could be concluded that overexpression of UCH-L1 in spermatogonia does not directly induce apoptosis in these cells (nor in Sertoli cells). Because spermatocytes are genetically distinct from the original mother cell (spermatogonia), we speculate that the Tg mice are highly susceptible to spermatocyte apoptosis in vivo, with the inference that spermatocytes seem to be particularly sensitive to UCH-L1 overexpression in spermatogonia even though spermatocytes themselves express a much lower level of UCH-L1. In contrast, *gad* mice are resistant to cryptorchid-induced germ cell apoptosis, and many germ cells undergo apoptosis in older animals although their testes develop nearly normally and produce mature sperm (Kwon et al., 2004b). These data suggest that the lack of UCH-L1 causes mice to have lower sensitivity to stress compared with wild-type males, although UCH-L1 is probably not essential for spermatogenesis under normal conditions. On one hand, UCH-L1 seems to be necessary for the stabilization of germ cells to protect against aging-associated apoptosis; however, the stabilization of germ cells appears to be limited by the concentration of UCH-L1, and consequently they may be damaged during spermatocyte meiosis when UCH-L1 is overexpressed. Despite the fact that excess UCH-L1 does not induce spermatogonial apoptosis, abnormalities in intracellular regulatory factors may potentially influence mitosis directly (i.e., as the cell divides into two daughter cells—spermatocytes). Some of these factors may accumulate or be reduced in the presence of excess UCH-L1, thereby causing disruptions such as arrested meiosis or the onset of apoptosis in spermatocytes rather than spermatogonia (Fig. 8).

Many of the factors involved in cellular apoptosis, including the Bcl-2 family and caspases, are targets for ubiquitynation. Previously, we have shown that Bcl-2 is upregulated (Kwon et al., 2004b) and caspases-3 is downregulated (Kwon et al., 2005) in *gad* mice. The decreased level of Bcl-2 and increased level of caspases-3

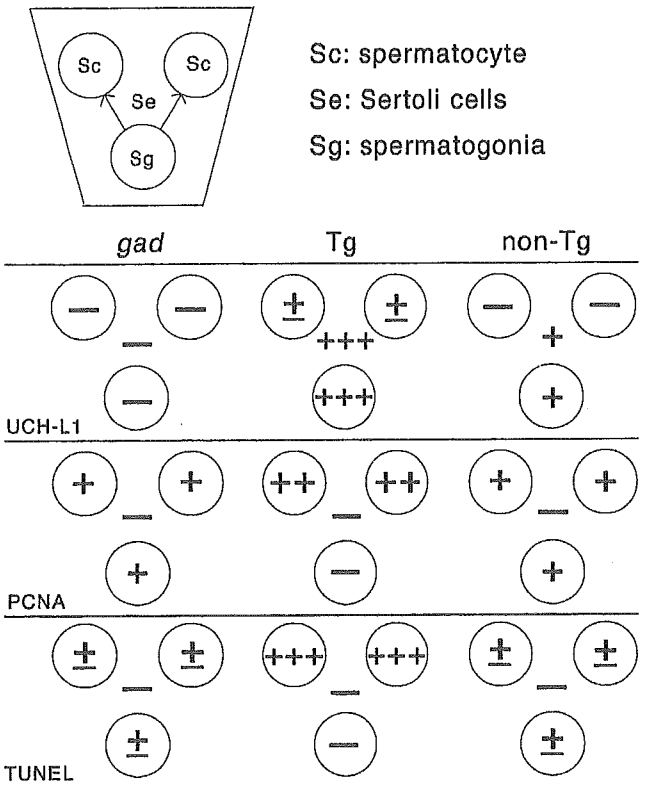


**Fig. 8.** TUNEL activity, and UCH-L1 and PCNA immunoreactivities in seminiferous tubules of non-Tg, *gad* and Tg mice. TUNEL activity or immunoreactivity: +++, strong; ++, moderate; + to ±, low to weak; –, not detectable.

observed in Tg mice in this study suggest that UCH-L1 can regulates the apoptosis during spermatogenesis by influencing the balance between apoptotic and anti-apoptotic proteins.

PCNA is ubiquitylated at lysine 48 (K48) and degraded by the ubiquitin-proteasome system (Yamamoto et al., 2004). In addition, PCNA is also monoubiquitylated at K164, thereby priming K63-linked polyubiquitin chains, which unlike K48-linked chains, do not promote proteasomal degradation (Hoege et al., 2002). In our present study, excess UCH-L1 relocalized PCNA from spermatogonia to spermatocytes and Sertoli cells in vivo and reduced PCNA expression to a low level in vitro. Based on these data, we hypothesize that UCH-L1, at least in part, may influence germ cell meiosis by affecting PCNA ubiquitynation, thereby disrupting its localization. In fact, PCNA significantly accumulated in primary spermatocytes of Tg mice (Fig. 4F). Since we did not obtain data regarding PCNA ubiquitylation in Tg mice, it is not clear whether the accumulated PCNA we observed was monoubiquitylated or polyubiquitylated. In any case, the accumulation of PCNA in primary spermatocytes may alter, damage or interrupt physical functions during meiosis (Fig. 8).

Germ cells and Sertoli cells are the only cell types expressed inside seminiferous tubules (McLaren, 1998). Germ cells constitute the male meiotic contribution to the reproductive cycle, whereas Sertoli cells support the growth and differentiation of germ cells. Direct interaction between germ cells and Sertoli cells may constitute an important part of the regulation of spermatogenesis (Russell et al., 1993). Indeed, mice exposed to Sertoli cell toxicants exhibit increased germ cell apoptosis (Lee et al., 1999). Therefore, Sertoli cells play a special role in nurturing and controlling spermatogenesis. Until postnatal day 16, UCH-L1 localizes only to spermatogonia, whereas after day 30 it also appears in Sertoli cells (Kon et al., 1999). Therefore, although UCH-L1 is highly expressed in both spermatogonia and somatic Sertoli cells, its function may be cell type-dependent. Under normal conditions UCH-L1 is a marker for activated Sertoli cells, in which it plays an important role in the degradation of abnormal proteins via the ubiquitin-proteasome system (Kon et al., 1999). Thus, we suspect that germ cell apoptosis in Tg mice might be related to the abnormal physical conditions in these cells. Our present work demonstrates that Tg mouse Sertoli cells are intensely immunoreactivity for UCH-L1, as expected. Furthermore, with vimentin, which is a marker present only in Sertoli cells (Oke and Suarez-Quian, 1993; Mori et al., 1997), we showed in this study that Tg mice had more vimentin immunoreactivity than non-Tg or *gad* mice (Fig. 5). Thus, forced expression of UCH-L1 in Sertoli cells perhaps may lead to gain of UCH function, thereby interrupting Sertoli cell-germ cell interactions that in turn promote germ cell apoptosis (Fig. 8).

In conclusion, we have demonstrated that UCH-L1 is an important spermatogenic factor related to PCNA and ubiquitin function. We used Tg mice overexpressing UCH-L1 to identify a new role for this protein. Overexpression of the *Uchl1* transgene inhibited spermatogenesis and induced germ cell death via an apoptotic mechanism, leading to male sterility. To our knowledge, the present data constitute the first description of a proapoptotic role for UCH-L1 in *Uchl1* Tg mice, as clearly revealed by the morphological and TUNEL results. Although UCH-L1 is constitutively expressed during spermatogenesis, and spermatogenic cell apoptosis is a normal aspect of mammalian spermatogenesis (Allan et al., 1992; Furuchi et al., 1996), the frequent cell death found in our *Uchl1* Tg mice could reflect an exaggeration of naturally occurring apoptosis. However, at present we do not understand whether the *Uchl1* transgene acts solely by inducing apoptosis or by interfering with differentiation so as to cause germ cell loss. This issue must be addressed to more fully define the role of UCH-L1 in the regulation and fate of spermatogonia during spermatogenesis.

## ACKNOWLEDGMENTS

We thank H. Kikuchi for assistance in preparing the sections and M. Shikama for the care and breeding of animals.

## REFERENCES

Allan DJ, Harmon BV, Roberts SA. 1992. Spermatogonial apoptosis has three morphologically recognizable phases and shows no circadian

rhythm during normal spermatogenesis in the rat. Cell Prolif 25: 241–250.

Aoki S, Su Q, Li H, Nishikawa K, Ayukawa K, Hara Y, Namikawa K, Kiryu-Seo S, Kiyama H, Wada K. 2002. Identification of an axotomy-induced glycosylated protein, AIGP1, possibly involved in cell death triggered by endoplasmic reticulum-Golgi stress. J Neurosci 22: 10751–10760.

Baarends WM, van der Laan R, Grootegoed JA. 2000. Specific aspects of the ubiquitin system in spermatogenesis. J Endocrinol Invest 23: 597–604.

Furuchi T, Masuko K, Nishimune Y, Obinata M, Matsui Y. 1996. Inhibition of testicular germ cell apoptosis and differentiation in mice misexpressing Bcl-2 in spermatogonia. Development 122: 1703–1709.

Harada T, Harada C, Wang YL, Osaka H, Amanai K, Tanaka K, Takizawa S, Setsuie R, Sakurai M, Sato Y, Noda M, Wada K. 2004. Role of ubiquitin carboxy terminal hydrolase-L1 in neural cell apoptosis induced by ischemic retinal injury in vivo. Am J Pathol 164:59–64.

Hoege C, Pfander B, Moldovan GL, Pyrowolakis G, Jentsch S. 2002. RAD6-dependent DNA repair is linked to modification of PCNA by ubiquitin and SUMO. Nature 419:135–141.

Hofmann MC, Narisawa S, Hess RA, Millan JL. 1992. Immortalization of germ cells and somatic testicular cells using the SV40 large T antigen. Exp Cell Res 201:417–435.

Imai T, Kawai Y, Tadokoro Y, Yamamoto M, Nishimune Y, Yomogida K. 2004. In vivo and in vitro constant expression of GATA-4 in mouse postnatal Sertoli cells. Mol Cell Endocrinol 214:107–115.

Kelman Z. 1997. PCNA: Structure, functions, and interactions. Oncogene 14:629–640.

Kon Y, Endoh D, Iwanaga T. 1999. Expression of protein gene product 9.5, a neuronal ubiquitin C-terminal hydrolase, and its developing change in sertoli cells of mouse testis. Mol Reprod Dev 54:333–341.

Kroll KL, Amaya E. 1996. Transgenic *Xenopus* embryos from sperm nuclear transplantations reveal FGF signaling requirements during gastrulation. Development 122:3173–3183.

Kurihara LJ, Kikuchi T, Wada K, Tilghman SM. 2001. Loss of Uch-L1 and Uch-L3 leads to neurodegeneration, posterior paralysis, and dysphagia. Hum Mol Genet 10:1963–1970.

Kwon J, Kikuchi T, Setsuie R, Ishii Y, Kyuwa S, Yoshikawa Y. 2003. Characterization of the testis in congenitally ubiquitin carboxy-terminal hydrolase-1 (Uch-L1) defective (gad) mice. Exp Anim 52: 1–9.

Kwon J, Wang YL, Setsuie R, Sekiguchi S, Sakurai M, Sato Y, Lee WW, Ishii Y, Kyuwa S, Noda M, Wada K, Yoshikawa Y. 2004a. Developmental regulation of ubiquitin C-terminal hydrolase isozyme expression during spermatogenesis in mice. Biol Reprod 71: 515–521.

Kwon J, Wang YL, Setsuie R, Sekiguchi S, Sato Y, Sakurai M, Noda M, Aoki S, Yoshikawa Y, Wada K. 2004b. Two closely related ubiquitin C-terminal hydrolase isozymes function as reciprocal modulators of germ cell apoptosis in cryptorchid testis. Am J Pathol 165:1367–1374.

Kwon J, Mochida K, Wang YL, Sekiguchi S, Sankai T, Aoki S, Ogura A, Yoshikawa Y, Wada K. 2005. Ubiquitin C-terminal hydrolase L-1 is essential for the early apoptotic wave of germinal cells and for sperm quality control during spermatogenesis. Biol Reprod 73:29–35.

Lee J, Richburg JH, Shipp EB, Meistrich ML, Boekelheide K. 1999. The Fas system: A regulator of testicular germ cell apoptosis, is differentially up-regulated in Sertoli cell versus germ cell injury of the testis. Endocrinology 140:852–858.

Matzuk MM, Lamb DJ. 2002. Genetic dissection of mammalian fertility pathways. Nat Cell Biol 4:s41–s49.

McLaren A. 1998. Gonad development: Assembling the mammalian testis. Curr Biol 8:R175–R177.

Mizushima S, Nagata S. 1990. pEF-BOS: A powerful mammalian expression vector. Nucleic Acids Res 18:5322.

Mori C, Nakamura N, Dix DJ, Fujioka M, Nakagawa S, Shiota K, Eddy EM. 1997. Morphological analysis of germ cell apoptosis during postnatal testis development in normal and Hsp 70-2 knockout mice. Dev Dyn 208:125–136.

Oke BO, Suarez-Quian CA. 1993. Localization of secretory, membrane-associated, and cytoskeletal proteins in rat testis using an improved immunocytochemical protocol that employs polyester wax. Biol Reprod 48:621–631.

Osaka H, Wang YL, Takada K, Takizawa S, Setsuie R, Li H, Sato Y, Nishikawa K, Sun YJ, Sakurai M, Harada T, Hara Y, Kimura I, Chiba S, Namikawa K, Kiyama H, Noda M, Aoki S, Wada K. 2003. Ubiquitin carboxy-terminal hydrolase L1 binds to and stabilizes monoubiquitin in neuron. Hum Mol Genet 12:1945–1958.

Osawa Y, Wang YL, Osaka H, Aoki S, Wada K. 2001. Cloning, expression, and mapping of a mouse gene, *Uchl4*, highly homologous to human and mouse Uchl3. Biochem Biophys Res Commun 283: 627–633.

Rasoulpour RJ, Schoenfeld HA, Gray DA, Boekelheide K. 2003. Expression of a K48R mutant ubiquitin protects mouse testis from cryptorchid injury and aging. Am J Pathol 163:2595–2603.

Russell LD, Corbin TJ, Borg KE, De Franca LR, Grasso P, Bartke A. 1993. Recombinant human follicle-stimulating hormone is capable of exerting a biological effect in the adult hypophysectomized rat by reducing the numbers of degenerating germ cells. Endocrinology 133:2062–2070.

Saigoh K, Wang YL, Suh JG, Yamanishi T, Sakai Y, Kiyosawa H, Harada T, Ichihara N, Wakana S, Kikuchi T, Wada K. 1999. Intragenic deletion in the gene encoding ubiquitin carboxy-terminal hydrolase in gad mice. Nat Genet 23:47–51.

Sutovsky P. 2003. Ubiquitin-dependent proteolysis in mammalian spermatogenesis, fertilization, and sperm quality control: Killing three birds with one stone. Microsc Res Tech 61:88–102.

Tokunaga Y, Imai S, Torii R, Maeda T. 1999. Cytoplasmic liberation of protein gene product 9.5 during the seasonal regulation of spermatogenesis in the monkey (*Macaca fuscata*). Endocrinology 140:1875–1883.

Toschi L, Bravo R. 1988. Changes in cyclin/proliferating cell nuclear antigen distribution during DNA repair synthesis. J Cell Biol 107: 1623–1628.

Wilkinson KD. 2000. Ubiquitination and deubiquitination: Targeting of proteins for degradation by the proteasome. Semin Cell Dev Biol 11:141–148.

Williams K, Schwartz A, Corey S, Orandle M, Kennedy W, Thompson B, Alvarez X, Brown C, Gartner S, Lackner A. 2002. Proliferating cellular nuclear antigen expression as a marker of perivascular macrophages in simian immunodeficiency virus encephalitis. Am J Pathol 161:575–585.

Wing SS. 2003. Deubiquitinating enzymes—the importance of driving in reverse along the ubiquitin-proteasome pathway. Int J Biochem Cell Biol 35:590–605.

Yamamoto T, Kimura S, Mori Y, Oka M, Ishibashi T, Yanagawa Y, Nara T, Nakagawa H, Hashimoto J, Sakaguchi K. 2004. Degradation of proliferating cell nuclear antigen by 26S proteasome in rice (*Oryza sativa* L.). Planta 218:640–646.

Yamazaki K, Wakasugi N, Tomita T, Kikuchi T, Mukoyama M, Ando K. 1988. Gracile axonal dystrophy (GAD): A new neurological mutant in the mouse. Proc Soc Exp Biol Med 187:209–215.

Yuan L, Liu JG, Zhao J, Brundell E, Daneholt B, Hoog C. 2000. The murine *SCP3* gene is required for synaptonemal complex assembly, chromosome synapsis, and male fertility. Mol Cell 5:73–83.

# Ubiquitin C-terminal hydrolase L1 regulates the morphology of neural progenitor cells and modulates their differentiation

Mikako Sakurai[1,2], Koichi Ayukawa[1], Rieko Setsuie[1,2], Kaori Nishikawa[1], Yoko Hara[1], Hiroki Ohashi[1,3], Mika Nishimoto[1,4], Toshiaki Abe[3], Yoshihisa Kudo[4], Masayuki Sekiguchi[1], Yae Sato[1,2], Shunsuke Aoki[1], Mami Noda[2] and Keiji Wada[1,*]

[1]Department of Degenerative Neurological Diseases, National Institute of Neuroscience, National Center of Neurology and Psychiatry, Kodaira, Tokyo, 187-8502, Japan
[2]Laboratory of Pathophysiology, Graduate School of Pharmaceutical Sciences, Kyushu University, Higashi-ku, Fukuoka, 812-8582, Japan
[3]Department of Neurosurgery, Graduate School of Medicine, Jikei University School of Medicine, Minato-ku, Tokyo, 105-8461, Japan
[4]Laboratory of Cellular Neurobiology, Tokyo University of Pharmacy and Life Science, Hachioji, Tokyo, 192-0392, Japan
*Author for correspondence (e-mail: wada@ncnp.go.jp)

*Accepted 27 September 2005*
*Journal of Cell Science 119, 162-171 Published by The Company of Biologists 2006*
*doi:10.1242/jcs.02716*

## Summary

**Ubiquitin C-terminal hydrolase L1 (UCH-L1) is a component of the ubiquitin system, which has a fundamental role in regulating various biological activities. However, the functional role of the ubiquitin system in neurogenesis is not known. Here we show that UCH-L1 regulates the morphology of neural progenitor cells (NPCs) and mediates neurogenesis. UCH-L1 was expressed in cultured NPCs as well as in embryonic brain. Its expression pattern in the ventricular zone (VZ) changed between embryonic day (E) 14 and E16, which corresponds to the transition from neurogenesis to gliogenesis. At E14, UCH-L1 was highly expressed in the ventricular zone, where neurogenesis actively occurs; whereas its expression was prominent in the cortical plate at E16. UCH-L1 was very weakly detected in the VZ at E16, which corresponds to the start of gliogenesis. In cultured proliferating NPCs, UCH-L1 was co-expressed with nestin, a marker of undifferentiated cells. In differentiating cells, UCH-L1 was highly co-expressed with the early neuronal marker TuJ1. Furthermore, when UCH-L1 was induced in nestin-positive progenitor cells, the number and length of cellular processes of the progenitors decreased, suggesting that the progenitor cells were differentiating. In addition, NPCs derived from *gad* (UCH-L1-deficient) mice had longer processes compared with controls. The ability of UCH-L1 to regulate the morphology of nestin-positive progenitors was dependent on its binding affinity for ubiquitin but not on hydrolase activity; this result was also confirmed using *gad*-mouse-derived NPCs. These results suggest that UCH-L1 spatially mediates and enhances neurogenesis in the embryonic brain by regulating progenitor cell morphology.**

Key words: PGP9.5, UCH-L1, Nestin, Ubiquitin, Cell morphology, Differentiation, Progenitor

## Introduction

Ubiquitin C-terminal hydrolase L1 (UCH-L1) is a member of the deubiquitylating enzymes and is one of the most abundant proteins in the brain. Whereas other UCH members are ubiquitously expressed, UCH-L1 is selectively expressed in neurons and testes/ovaries in the adult (Wilkinson et al., 1989). UCH-L1 is also known as PGP9.5 and is used as a neuron-specific marker in neuroanatomical and neuropathological studies (Dickson et al., 1994; McQuaid et al., 1995). Recent studies suggest that UCH-L1 is involved in neurodegeneration. The I93M mutation and the S18Y polymorphism in UCH-L1 are implicated in Parkinson's disease (Leroy et al., 1998; Satoh and Kuroda, 2001). Using gracile axonal dystrophy (*gad*) mice, we previously demonstrated that the dying-back type of axonal degeneration is caused by a deletion of the *Uchl1* gene (Saigoh et al., 1999). UCH-L1 has an affinity for ubiquitin and ensures its stability within neurons in vivo (Osaka et al., 2003). Furthermore, UCH-L1 has ubiquitin ligase activity (Liu et al., 2002). Thus, UCH-L1 might have multiple functions and more roles in biological phenomena than previously expected.

UCH-L1 mRNA is first detected at embryonic day (E) 8.5-9 in the neural tube and in the neural epithelium (Schofield et al., 1995). In addition, UCH-L1 immunoreactivity has been observed in the neural tube at E10.5 (Sekiguchi et al., 2003). However, its functional role in embryonic neurogenesis is not well understood. CDK5 and Dab1 are involved in regulating the migratory behavior of postmitotic neurons. Both p35, which is a CDK5 kinase, and Dab1 are degraded by the ubiquitin-proteasome pathway (Arnaud et al., 2003; Bock et al., 2004; Patrick et al., 1998). Thus, the ubiquitin system might be important in the migration and differentiation of postmitotic neurons and for the lamination pattern of the cerebral cortex.

Neural progenitor cells (NPCs) differentiate into neurons, astrocytes and oligodendrocytes (Qian et al., 1998; Qian et al., 2000; Shen et al., 1998). In the embryonic brain, neuroepithelial cells and radial glia are present in the ventricular zone (VZ); neurogenesis occurs first, followed by

gliogenesis. Committed progenitor cells move from the VZ to the cortical plate (CP) (Noctor et al., 2004). The differentiating cells migrate by means of radial migration, during which the migrating cells change their morphology (Kawauchi et al., 2003; Noctor et al., 2002; Tabata and Nakajima, 2003). Here, we analyzed the functional role of UCH-L1 using mouse embryonic NPCs. Our results indicate that UCH-L1 is expressed in nestin-positive NPCs and might regulate neurogenesis. The expression pattern of UCH-L1 changed in parallel with the transition from neuronal generation to glial generation. Furthermore, UCH-L1 modulated the length of nestin-positive processes in NPCs. Our results constitute the first evidence that UCH-L1 is important in neurogenesis and thus provide the basis for further investigation into the role of the ubiquitin system in neurogenesis.

## Results

### UCH-L1 expression in embryonic mouse brain

We first determined the specificity of the UCH-L1 antibody using immunoblotting (data not shown) and immunostaining. Because *gad* mice do not express endogenous UCH-L1 (Saigoh et al., 1999), we used these mice as a negative control. Heterozygous littermates had UCH-L1 immunostaining, whereas UCH-L1 immunoreactivity was not detected in the brains of *gad* mice (Fig. 1). These results confirmed the specificity of the antibody against UCH-L1. Using this antibody, we further compared the distribution and expression of UCH-L1 with the neural progenitor marker nestin and the early neuronal marker TuJ1. Nestin was expressed in the VZ of brains from both *gad* and heterozygous mice at E13 (Fig. 1). Nestin expression was observed throughout the region, whereas TuJ1 immunoreactivity was detected at the marginal zone (MZ). In heterozygous mice, UCH-L1 and nestin immunostaining overlapped in almost all cells in the VZ, suggesting that UCH-L1 is expressed in NPCs (Fig. 1A). TuJ1 expression colocalized with that of UCH-L1 in MZ cells, indicating that UCH-L1 is expressed in embryonic neurons as well (Fig. 1B). In E13 *gad* mouse brain, nestin staining differed compared with that in heterozygous littermates. Nestin staining was observed in many long radial fibers in the mutant, which we believed were radial glia; by contrast, staining in the heterozygotes occurred in radial glia as well as in neuronal cells at various stages of development (Fig. 1A; arrow and arrowhead).

We then looked for developmental changes in UCH-L1 expression. In the embryonic cerebral cortex, asymmetric cell division generates one neuron and one neural progenitor (Roegiers and Jan, 2004; Zhong et al., 1996; Zhong et al., 1997). These asymmetric cell divisions begin at E11, peak around E14, and subside after E16. At E14, astrocytes and oligodendrocytes are not yet present. However, at E16, glial cell production begins. The regional expression level for both nestin and TuJ1 did not change between E14 and E16 (Fig. 2A,B). At E14 and E16, nestin immunoreactivity was stronger in the VZ (Fig. 2A) and was faintly detected only along radial glial fibers in the CP (Fig. 2A,C; arrowhead) (Malatesta et al., 2003; Malatesta et al., 2000). TuJ1 immunoreactivity was predominantly detected in the MZ, CP, intermediate zone and subventricular zone at E14 and E16 (Fig. 2B,D). In the VZ, TuJ1 immunoreactivity was detected only in migrating neurons (Fig. 2D; arrowhead).

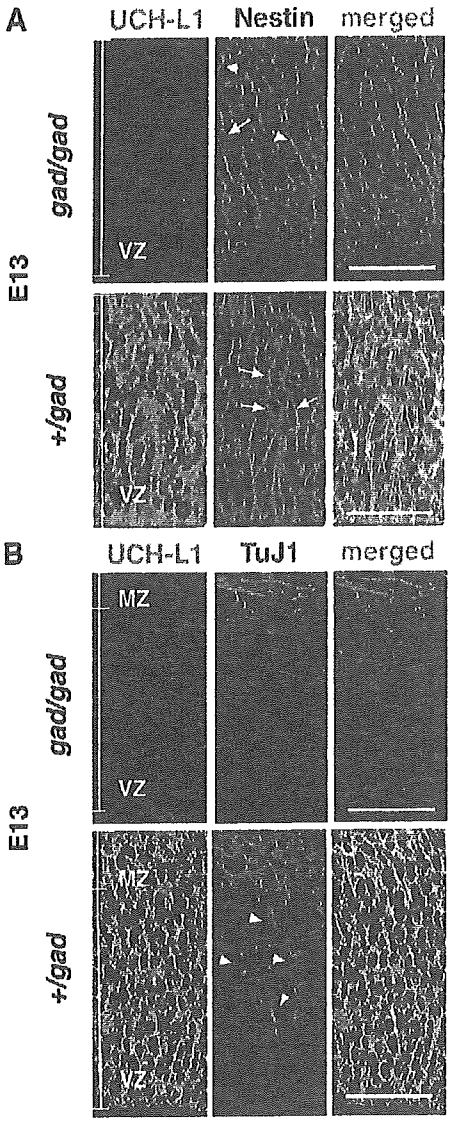


**Fig. 1.** Antibody specificity and expression of UCH-L1 in the ventricular zone at E13. UCH-L1 expression was detected using immunohistochemistry with anti-PGP9.5. UCH-L1 is not detected in the brain of *gad* mice at E13 (A,B) but is strongly expressed in heterozygous littermates (A,B). Confocal microscopic images of coronal sections of *gad* mice and heterozygous littermates were double stained with antibodies for the progenitor marker nestin and UCH-L1 (PGP9.5) (A) or for the early neuronal marker tubulin β III (TuJ1) and UCH-L1 (B). Long radial fibers are indicated by arrowheads, and various phases of progenitor cells are indicated by arrows (A). TuJ1-positive, migrating neuronal cells are indicated by arrowheads (B). MZ, marginal zone; VZ, ventricular zone. Bars, 40 μm.

By contrast, the pattern of UCH-L1 expression changed between E14 and E16 (Fig. 2A,B). At both stages of development, UCH-L1 was expressed in neuronal cells as well as in progenitor cells. UCH-L1 immunoreactivity was stronger in the VZ than in the CP at E14; however, the immunoreactivity

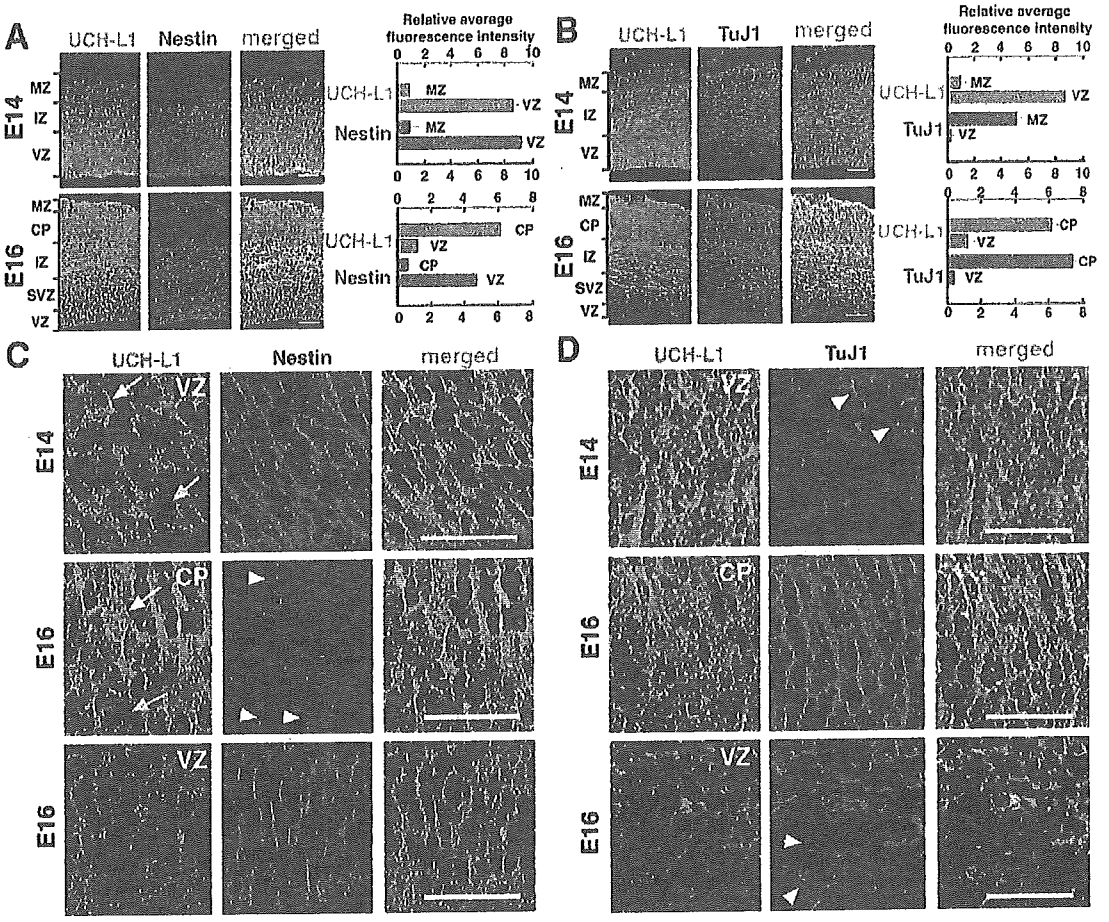


**Fig. 2.** Change in UCH-L1 expression pattern in the developing mouse brain. Cryosections of the brain at E14 and E16 were double stained with UCH-L1 and the neural progenitor marker nestin (A) or early neuronal marker TuJ1 (B). Unlike with UCH-L1, staining patterns for TuJ1 and nestin do not change between E14 and E16. At E14, UCH-L1 expression is higher in the VZ than in the MZ. At E16, higher expression of UCH-L1 is reciprocally detected in the CP. By contrast, at both E14 and E16, nestin is highly expressed in the VZ, and TuJ1 expression is higher in the MZ/CP. Fluorescence intensities per field (1700 $\mu m^2$) were measured in each layer of the E14 and E16 brain and are shown to the right. Bars, 80 μm. (C,D) Higher-magnification images from A,B of UCH-L1 expression in the E14 and E16 brain: UCH-L1 and nestin (C); UCH-L1 and TuJ1 (D). UCH-L1 and nestin are co-expressed in the VZ at E14 and E16. Nestin is expressed only in radial glial fibers (arrowheads) of the CP but not in neurons. UCH-L1 expression level is high. A representative cell with a high level of UCH-LI expression is indicated by a white arrow and one with low expression is indicated by a yellow arrow (C). An early neuronal marker, TuJ1, was expressed in both migrating (arrowheads) and mature neurons (D). CP, cortical plate; IZ, intermediate zone; MZ, marginal zone; SVZ, subventricular zone; VZ, ventricular zone. Bars, 40 μm.

was stronger in the CP than in the VZ at E16 (Fig. 2A,B). The regional change in UCH-L1 expression between E14 and E16 was further confirmed by measuring immunofluorescence intensities from confocal images of the MZ/CP and VZ. At E14, the relative UCH-L1 expression level in the VZ was 9.3 times higher than that in the MZ (Fig. 2A).

Conversely, at E16, when neuronal maturation occurs in the CP, UCH-L1 immunoreactivity in the CP was 5.0 times higher than in the VZ (Fig. 2B). UCH-L1 immunoreactivity colocalized with that of nestin in the VZ at both E14 and E16, although UCH-L1 expression in the VZ was lower at E16 (Fig. 2C). In the VZ at E14, nestin was expressed homogeneously; however, the pattern of UCH-L1 immunoreactivity was mixed, with strong and weak intensities (Fig. 2C; arrow). This expression pattern might reflect the heterogeneity of progenitor cells. Nestin-positive radial glial fibers were observed in the CP at E16 through mature neurons, which strongly expressed UCH-L1 (Fig. 2C) (Malatesta et al., 2000; Malatesta et al., 2003).

## UCH-L1 and nestin expression in cultured NPCs

Because areas of nestin and UCH-L1 immunoreactivity overlapped in the VZ, where NPCs reside, we subsequently analyzed the transition of UCH-L1 expression using cultured NPCs. We performed double-labeling experiments for UCH-L1 and nestin expression in cultured NPCs. In the presence of basic fibroblast growth factor (bFGF), when NPCs are proliferating, the percentage of UCH-L1/nestin double-positive

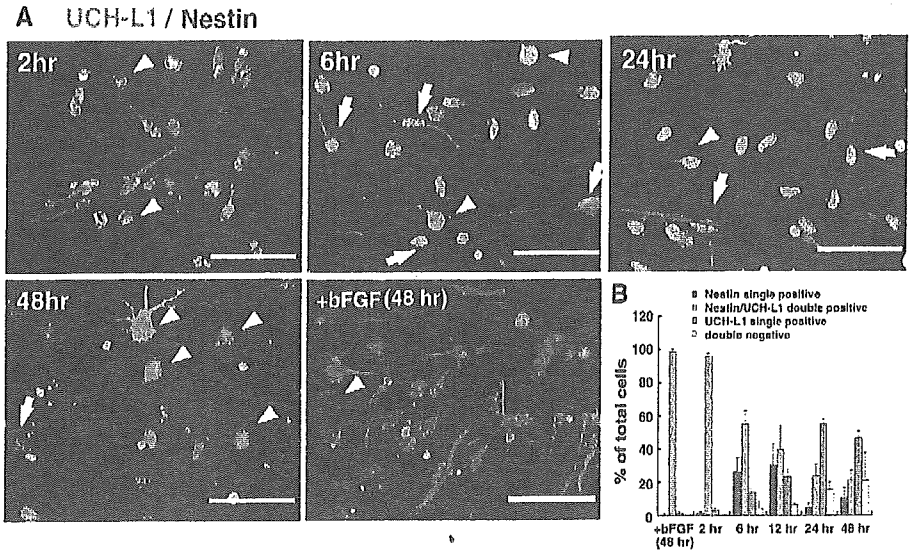


**Fig. 3.** Nestin and UCH-L1 expression in undifferentiated and differentiating NPCs at 2, 6, 12, 24 and 48 hours. (A) NPCs were immunolabeled with antibodies against nestin and UCH-L1 in the proliferating phase (+bFGF; at 48 hours) or the differentiation phase (–bFGF; 2, 6, 24, 48 hours). Cultures were counterlabeled with Hoechst nuclear dye to facilitate cell quantification. (B) Quantitative analysis of the percentage of cells stained with each antibody. Nestin-positive cells gradually decrease as differentiation proceeds. The UCH-L1 expression level is both high (arrowheads) and low (arrows) in nestin-positive cells at 6 hours. Each experiment was analyzed by counting cells in three independent wells at the indicated times. The experiments were repeated at least two times. Bars, 50 μm.

cells did not change 48 hours after plating, and almost all NPCs expressed UCH-L1 (Fig. 3A). The majority (97.5±2.2%; mean±s.d.) of cultured cells were nestin positive and most of them also stained for UCH-L1 2 hours after plating without bFGF, which triggers NPC differentiation. UCH-L1/nestin double-positive cells were detected at all time points, but as differentiation proceeded their numbers gradually decreased from 95.8±1.9% at 2 hours to 21.5±5.8% at 48 hours (Fig. 3A,B). Although UCH-L1 single-positive cells were rarely detected at 2 hours, the population increased with differentiation, and by 24 hours after bFGF removal 55.1±2.9% of cultured cells were UCH-L1 single-positive cells. Conversely, nestin single-positive cells were readily detected during the earlier phase of differentiation, especially at 6 hours (26.4±8.4% of total cells) and 12 hours (27.0±14.0% of total cells). The differentiating NPCs included nestin-positive cells in which UCH-L1 was either strongly or weakly expressed (Fig. 3A; arrow and arrowhead at 6 hours). These data indicate that UCH-L1 is expressed in progenitor cells as well as in differentiating NPCs. Nestin-positive cells can probably be

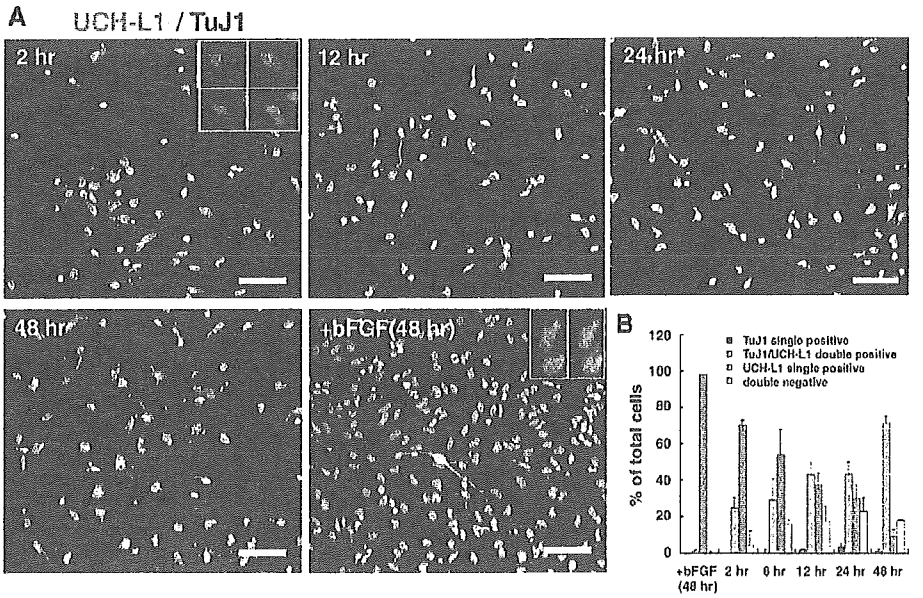


**Fig. 4.** UCH-L1 expression in neurogenesis. NPCs were immunolabeled with antibodies against TuJ1 and UCH-L1. Cultures were counterlabeled with Hoechst nuclear dye to facilitate cell quantification. Quantitative analysis of the percentage of cells stained with each antibody. (A) In the proliferating phase (+bFGF; at 48 hours) or the differentiation phase (–bFGF; 2, 12, 24, 48 hours), most TuJ1-positive cells co-express UCH-L1. The UCH-L1 expression level is both high and low in TuJ1-positive cells at 48 hours. (B) Quantitative analysis of the percentage of cells stained with each antibody. The number of TuJ1-positive cells gradually increased in the differentiating phase (–bFGF; B). Each experiment was analyzed by counting cells in three independent wells at the indicated times. The experiments were repeated at least two times. Bars, 50 μm.

categorized into at least two subgroups based on their UCH-L1 expression (Fig. 3A,B).

### UCH-L1 and TuJ1 expression in cultured NPCs

We then analyzed the expression patterns of UCH-L1 and TuJ1. In the presence of bFGF, TuJ1-positive cells were rarely detected. However, in the absence of bFGF, TuJ1-positive cells were induced. In the cultures without bFGF, as the UCH-L1 single-positive cell population decreased with time, the UCH-L1/TuJ1 double-positive population increased (Fig. 4A,B). UCH-L1/TuJ1 double-negative cells were detected in the differentiating phases at 6, 12, 24 and 48 hours. UCH-L1/TuJ1 double-negative cells might be the nestin single-positive cells at 6 hours and 12 hours in Figs 3 and 4. TuJ1 single-positive cells were infrequently detected in the differentiating NPCs. Because 71.4±3.4% of NPCs differentiated into TuJ1-positive cells under our culture conditions without bFGF at 48 hours, almost all UCH-L1-positive cells are thought to differentiate into TuJ1-positive neuronal cells (Fig. 4A,B). The differentiating NPCs included TuJ1-positive cells in which UCH-L1 was either strongly or weakly expressed (Fig. 4A). These data indicate that UCH-L1-positive NPCs have a high potential for differentiating into neuronal cells and that TuJ1-positive neuronal cells are heterogeneous with regard to UCH-L1 expression.

### Morphological classification of UCH-L1-positive NPCs

Nestin is a marker of undifferentiated cells, whereas UCH-L1 is a neuron-specific marker. Here, UCH-L1/nestin double-positive cells were present in cultured NPCs as well as in embryonic brain (Figs 2, 3). Cultured NPCs sequentially gave rise to neurons, then astrocytes, and finally oligodendrocytes (data not shown). Under our culture conditions, neurogenesis actively occurred in differentiating NPCs between 2 and 12 hours after plating (Fig. 4). Glial differentiation had not begun by this time. We collected differentiating NPCs at 6 hours and 12 hours after plating and then analyzed the morphology of nestin-positive cells (Fig. 5). Both UCH-L1/nestin double-positive cells and nestin single-positive cells were present in the population of differentiating NPCs. As the population of double-positive cells might represent a progression of differentiating neurons, we examined the morphology of these cells. Differentiating neurons undergo a stereotypical set of morphological changes, including length (from long to short) (Fukuda et al., 2003; Hartfuss et al., 2003; Nadarajah et al., 2001). We categorized the nestin-positive cells with respect to process length (long, short or round; Fig. 3). UCH-L1 single-positive and double-negative cells were included in the total number of cells. When the total length of processes was more than four times the diameter of the nucleus of the cell, the cell was categorized as 'long', whereas cells with shorter processes were categorized as 'short'. Cells that did not have processes were classified as 'round'. At 6 hours, the majority of nestin single-positive cells were long (18.2±7.6% vs 4.0±0.2% short cells; mean±s.d.; Fisher's PLSD, $P$=0.008), whereas the majority of UCH-L1/nestin double-positive cells were short (62.0±6.3%). This population was significantly greater than that of long cells (10.3±2.0%) and round cells (5.0±1.7%; Fisher's PLSD, $P$<0.0001). When NPCs with processes were subcategorized as unipolar, bipolar or multipolar, the unipolar population was significantly higher (62.3±16.9%) than the bipolar population (18.2±3.9%; Fisher's PLSD, $P$=0.002) in UCH-L1/nestin double-positive cells. Multipolar cells were not observed at 12 hours. However, in nestin single-positive cells, more NPCs were bipolar (16.5±4.6%) than unipolar (4.5±1.9%; Fisher's PLSD, $P$=0.009; Fig. 6B). Similar results were obtained at 12 hours (Fig. 6). Thus, most UCH-L1/nestin double-positive cells had shorter processes and were more likely to be unipolar.

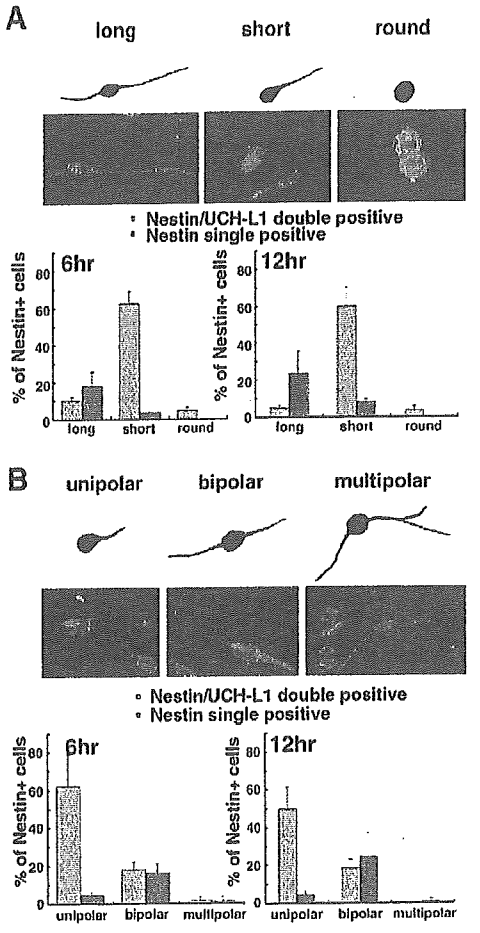


**Fig. 5.** Morphological identification of subpopulations of cultured NPCs at 6 and 12 hours after induction of differentiation. Differentiating NPCs were double stained with UCH-L1 and nestin. For the quantification depicted in A, differentiating NPCs stained with UCH-L1 and nestin were classified as long, short or round (see text). For the quantification depicted in B, differentiating NPCs were classified based on three kinds of cell morphology: unipolar, bipolar, or multipolar.

### Effect of UCH-L1 on nestin-positive processes

We next examined the effect of UCH-L1 on proliferating NPC morphology using the transient transfection method. NPCs were allowed to proliferate for 48 hours after transfection and were then induced to differentiate for 12 hours. The cells were fixed, and the length of nestin-positive processes was examined. To quantify the relationship between UCH-L1 expression and process formation, we measured the total length

of nestin-positive processes. Untransfected NPCs that were nestin positive had mainly long, bipolar processes (Fig. 3A, +bFGF). Cells that were transfected with a green fluorescent protein (GFP) expression vector (negative control) had a morphology that was similar to that of untransfected cells (Fig. 6A). By contrast, cells transfected with wild-type (WT) UCH-L1 cDNA had significantly shorter processes (47.6±6.4 μm, mean±s.e.m., $n$=81) than mock-transfected cells (69.9±7.0 μm, $n$=82) (Fig. 6A).

We then examined the relationship between the UCH-L1 structure and its activity with respect to morphological induction. We prepared two UCH-L1 mutants: D30A UCH-L1 lacked hydrolase activity and binding affinity for ubiquitin (Fig. 6B,C) (Osaka et al., 2003); C90S UCH-L1 lacked hydrolase activity but maintained binding affinity for ubiquitin (Fig. 6B,C) (Osaka et al., 2003). We compared the deubiquitylating activity of each UCH-L1 mutant using Ub-AMC as a substrate. The D30A mutant had little hydrolase activity, and the activity of the C90S mutant was not detectable (Fig. 6B; right). Sodium dodecyl sulfate-polyacrylamide gel electrophoresis revealed that there were no detectable contaminating proteins in these recombinant protein preparations (Fig. 6B; left). Co-immunoprecipitation experiments demonstrated that WT UCH-L1 and the C90S mutant physically associated with monoubiquitin. The D30A mutant (as well as GFP alone, which was used as a control) did not associate with ubiquitin (Fig. 6C). Although we did not detect a statistically significant difference, cells transfected with the D30A mutant tended to have longer nestin-positive processes (83.4±7.1 μm, $n$=87) as compared with cells transfected with the GFP expression vector (Fig. 6A). By contrast, cells transfected with the C90S mutant had significantly shorter fibers (39.3±4.5 μm, $n$=120; ANOVA: $F$=11.5, $P$<0.0001; Dunnett's multiple comparison test: GFP vs WT, $P$<0.05; GFP vs C90S, $P$<0.001; GFP vs D30A, $P$>0.05; Fig. 6A). We also compared the length of nestin-positive processes among UCH-L1 mutants (Bonferroni-Dunn Multiple Comparison Test: WT vs C90S, $P$=0.32; WT vs D30A, $P$<0.0001; D30A vs C90S, $P$<0.0001). Taken together, our data suggest that the effect of UCH-L1 expression on NPC morphology is dependent on the interaction between monoubiquitin and UCH-L1.

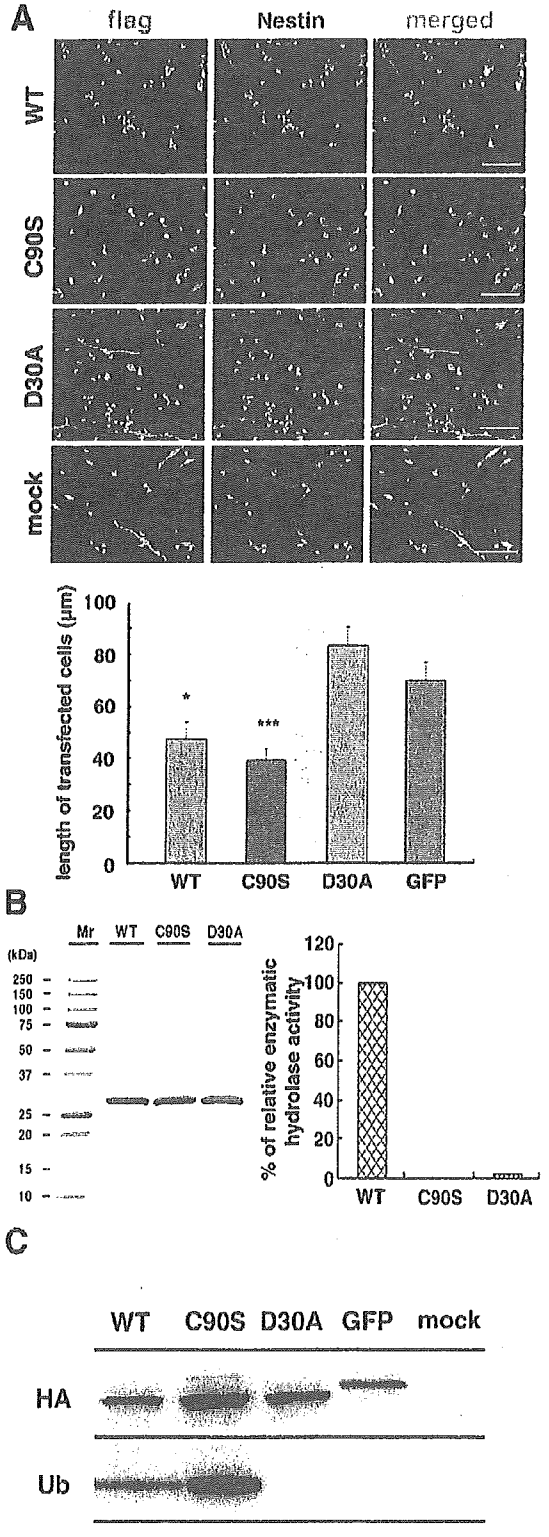


**Fig. 6.** The induction of short processes depends on the interaction between UCH-L1 and monoubiquitin. (A) FLAG-tagged WT UCH-L1, C90S UCH-L1, D30A UCH-L1 and GFP (all in the pCI-*neo* vector) were transfected into NPCs. Antibodies against the FLAG-tag were used to detect transfected UCH-L1. The green staining shows transfected cells and the red staining shows endogenous nestin. Transient transfection of each construct was performed under proliferating conditions. At 48 hours after transfection, bFGF was removed for 12 hours before the cultures were immunostained. The lengths of nestin-positive processes in immunostained cells were measured. Asterisks indicate differences from the value of GFP-transfected NPCs at *$P$<0.05 and ***$P$<0.001. Bars, 80 μm. (B) Visualization of recombinant 6HN-tagged UCH-L1 by sodium dodecyl sulfate-polyacrylamide gel electrophoresis with Coomassie staining (B, left). UCH-L1 hydrolase activity was measured by Ub-AMC hydrolysis. Enzyme concentration was 4.3 nM, and substrate concentration was 700 nM. Initial velocity data was used to determine the values for relative hydrolase activity of UCH-L1 (B, right). (C) UCH-L1 co-immunoprecipitated with Ub. Cytosolic extracts from NIH-3T3 cell lines stably expressing HA-tagged WT UCH-L1 and mutants thereof were immunoprecipitated using anti-HA and immunoblotted with anti-HA antibody or anti-Ub antibody.

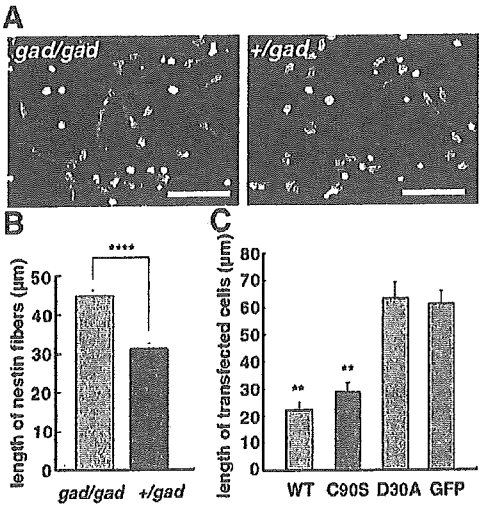


**Fig. 7.** A comparative experiment of *gad* mice and heterozygous littermates. The experiment compared *gad* mice (A,B) with a transfection study using FLAG-tagged WT UCH-L1, C90S UCH-L1, D30A UCH-L1 and GFP (mock) into *gad*-mouse-derived NPCs (C). The lengths of nestin-positive processes in immunostained cells were measured. NPCs from *gad* mice had longer nestin-positive processes compared with the control (A,B). (C) At 48 hours after transfection, bFGF was removed for 12 hours before the cultures were immunostained. The lengths of nestin-positive processes in immunostained cells were measured. Asterisks indicate differences from the value of GFP-transfected NPCs at $^{**}P<0.01$ and $^{****}P<0.0001$. Bar, 50 μm.

### A comparative experiment using *gad*-mouse-derived NPCs

We did a comparative experiment using *gad* mice and heterozygous littermates. Nestin-positive NPCs from *gad* mice had longer processes. When we measured the length of nestin-positive fibers, NPCs from *gad* mice (45.0±1.4 μm, mean±s.e.m., $n$=366) had significantly longer nestin-positive processes compared with the control (31.4±1.3 μm, $n$=363) (Mann-Whitney U test: *gad* vs control, $P<0.0001$; Fig. 7A,B).

We next examined the effect of UCH-L1 on *gad*-mouse-derived NPCs using the transient transfection method. As observed in B6-derived cells, NPCs from *gad* mice that were transfected with WT UCH-L1 cDNA had significantly shorter processes (22.2±2.7 μm, mean±s.e.m., $n$=70) than mock-transfected cells (61.0±4.9 μm, $n$=88) (Bonferroni-Dunn multiple comparison test: GFP vs WT, $P<0.0001$) (Fig. 7C). Similarly, cells transfected with the C90S mutant had significantly shorter fibers (28.9±3.1 μm, $n$=71) (GFP vs C90S, $P<0.0001$). Although we did not detect a statistically significant difference, cells transfected with the D30A mutant tended to have longer nestin-positive processes (63.3±5.9 μm, $n$=80) as compared with cells transfected with the GFP expression vector (GFP vs D30A, $P$=0.70) (Fig. 7C). We also compared the length of nestin-positive processes among UCH-L1 mutants (Bonferroni-Dunn multiple comparison test: WT vs C90S, $P$=0.32; WT vs D30A, $P<0.0001$; D30A vs C90S, $P<0.0001$). Taken together, our data suggest that the effect of UCH-L1 expression on NPC morphology is dependent on the interaction between monoubiquitin and UCH-L1.

## Discussion

UCH-L1 is a neuron-specific marker in the adult brain. In the present study, we provide experimental evidence that UCH-L1 is expressed in NPCs (Figs 2, 3). Using immunohistochemistry in the mouse brain, we detected UCH-L1 expression at E14 and E16. Interestingly, the expression pattern differed between E14 and E16 (Fig. 2). At E14, when the CP is forming, UCH-L1 expression was higher in the VZ than in the CP. At E14, the VZ contains progenitor cells that are generating neurons in the neocortex (Hashimoto and Mikoshiba, 2004; Malatesta et al., 2003). By contrast, UCH-L1 expression at E16 was lower in the VZ than in the CP. At E16, neuritogenesis and neuronal maturation are active in the CP, and gliogenesis is beginning in the VZ (Rice and Curran, 2001). The cerebral cortex layer becomes thicker at E16, where glial cells are not yet generated. The staining pattern for TuJ1 and nestin did not change between E14 and E16 (Fig. 2), indicating that UCH-L1 is highly expressed in the cortical layer prior to gliogenesis. The change in the expression pattern of UCH-L1 was coincident with the transition from neurogenesis to gliogenesis in the VZ. These results raise the possibility that UCH-L1 mediates not only the neuronal differentiation of NPCs but also the transition from neurogenesis to gliogenesis.

Time is a pivotal factor in the programmed sequence that produces neurons and glial cells from NPCs (Qian et al., 2000), in that the switch from neurogenesis to gliogenesis is regulated by time. The mechanism behind this progression of the progenitor cells is not well understood. Cultured NPCs generate neurons first, followed by astrocytes and then oligodendrocytes (Qian et al., 2000; Temple, 2001). This order of production for each population has been verified in vivo (Sauvageot and Stiles, 2002). The pattern of UCH-L1 immunoreactivity suggests that UCH-L1 is required for the onset of neurogenesis, which is followed by glial differentiation (Fig. 2).

We thus examined the role of UCH-L1 in neurogenesis using cultured NPCs. In UCH-L1/nestin double-staining experiments, the number of double-positive cells decreased with time in culture (Fig. 3). Conversely, UCH-L1 single-positive cells increased. In the double-staining experiments for UCH-L1 and TuJ1, the number of UCH-L1 single-positive cells decreased with time in culture, whereas the number of UCH-L1/TuJ1 double-positive cells increased (Fig. 4). These observations suggest that most UCH-L1-positive cells initially express nestin, but they express TuJ1 at a later stage. As we observed in vivo and in vitro (Figs 2-4), NPCs express UCH-L1, and its expression increases as the NPCs differentiate into neuronal cells. The number of nestin single-positive cells transiently increased before the UCH-L1 single-positive population increased (Fig. 3). The nestin single-positive population might have changed into the UCH-L1/nestin double-negative population (Fig. 3). Although the fate of the double-negative populations remains unknown, the double-negative cells might represent glial cells. Alternatively, some of the nestin single-positive cells might have changed into UCH-L1/nestin double-positive cells and then differentiated into UCH-L1 single-positive cells. A few UCH-L1-negative and TuJ1-positive cells were detected in the differentiating NPCs (Fig. 4). Thus, TuJ1-positive early neurons appear to be heterogeneous. UCH-L1/TuJ1 double-positive immunoreactivity suggested that UCH-L1 is not

absolutely required for some portion of neuronal cell development (Fig. 1B and Fig. 4A). This might explain why *gad* mouse neurons develop despite the absence of UCH-L1.

Because UCH-L1 was expressed in nestin-positive NPCs, we further examined the role of UCH-L1 in cell morphology (Fig. 5). Differentiating NPCs change morphology (Noctor et al., 2001), but the role of UCH-L1 in differentiating neurons has not been investigated. We classified nestin-positive cells based on the length of their processes. Nestin single-positive cells were predominantly long, whereas most UCH-L1/nestin double-positive cells were predominantly short (Fig. 5). These results suggest that UCH-L1 plays a role in regulating NPC process length. We examined this possibility by inducing UCH-L1 in nestin-positive cells. Untransfected, proliferating nestin-positive NPCs had mainly long and bipolar processes [Fig. 3A, bFGF (48 hours)], but when UCH-L1 was transfected, the length of nestin-positive NPC processes shortened (Fig. 6A). The unipolar population increased following UCH-L1 expression. These results support the idea that UCH-L1 regulates NPC morphology. This idea was further confirmed by observations in NPCs from *gad* mice; as shown in Fig. 7B, NPCs from homozygous *gad* mice had longer processes than those from heterozygous controls. In addition, we observed that transfection of UCH-L1 shortened the processes of NPCs from *gad* mice compared with mock transfectants (Fig. 7C).

Our results also suggest that at least two populations of NPCs exist in the embryonic brain. The populations can be classified by the presence or absence of UCH-L1. In the dentate gyrus of the adult mouse brain, there are two distinct subpopulations of nestin-positive cells (Fukuda et al., 2003): those having short processes differentiate into neurons, whereas those having long processes generate late progenitors, which have short processes. The nestin staining pattern of brains from *gad* mice differed from that of brains from heterozygous littermates (Fig. 1). In the *gad* mouse brain, nestin-positive radial fibers were prominent, and almost all progenitor cells appeared to have long processes (Fig. 1). Since UCH-L1 affected NPC morphology (Fig. 6A and Fig. 7C), the difference in vivo indicates that differentiation itself was modulated by the absence of UCH-L1. Considering that neurons are present in the *gad* mouse even though it lacks UCH-L1 expression, further investigation into the morphological role of UCH-L1 using various approaches including the BrdU studies should provide important information about the heterogeneity of cortical neurons.

UCHs hydrolyze ubiquitin C-terminal small adducts in vitro (Larsen et al., 1998). Recently, a significant relationship was reported between UCH-L1 hydrolase activity and cell proliferation in lung cancer cell lines (Liu et al., 2003). We previously demonstrated that UCH-L1 extends ubiquitin half-life and prevents ubiquitin degradation. This function depends on the interaction between UCH-L1 and monoubiquitin but not on hydrolase activity (Osaka et al., 2003). In the present study, WT UCH-L1 and the C90S mutant both decreased the length of NPC processes. Both molecules associate with monoubiquitin, unlike another mutant, D30A, which did not affect process length (Fig. 6). Similar results were obtained from the transfection study using nestin-positive NPCs from *gad* mice (Fig. 7C). Thus, the effect of UCH-L1 on NPC process length is dependent on the interaction between UCH-L1 and ubiquitin but not on hydrolase activity. Although we did not examine the ligase activity of each mutant (Liu et al., 2002), the C90S mutant is unlikely to have ligase activity, because conjugation of ubiquitin to the C90S mutant forms a stable complex that prevents the release of ubiquitin (Sullivan and Vierstra, 1993). This observation suggests that the ligase activity is not related to the morphological changes that occurred in NPCs.

The ubiquitin system has an essential role in various physiological events, including cell-cycle progression, specific gene transcription, membrane protein trafficking, reversal of stress damage and intracellular signaling (Weissman, 2001). In cortical neurogenesis, the role of the ubiquitin system is not well understood. Several molecules that are important in cortical neurogenesis, including Notch, P35 and Dab1, are ubiquitylated (Arnaud et al., 2003; Bock et al., 2004; Patrick et al., 1998; Qiu et al., 2000). Here we show for the first time that UCH-L1 is expressed in NPCs and regulates their morphology. In addition, in vivo UCH-L1 expression is localized to the VZ and cortical layers that are undergoing neurogenesis. Cells undergoing gliogenesis had little UCH-L1 expression in vivo. These results suggest that UCH-L1 facilitates neurogenesis, an activity that appears to depend on the affinity of UCH-L1 for ubiquitin.

## Materials and Methods

### Animals

Pregnant C57BL/6J mice were purchased from CLEA Japan. The *gad* mouse is an autosomal recessive mutant that was obtained by crossing CBA and RFM mice (Saigoh et al., 1999). The *gad* line was maintained by intercrossing for more than 20 generations (Kwon et al., 2003; Saigoh et al., 1999). All animal experiments were performed in the laboratory according to the NIH Standards for Treatment of Laboratory Animals.

### Antibodies and reagents

Monoclonal and polyclonal antibodies used in this study were as follows: monoclonal anti-nestin antibody (Becton Dickinson; and Rat401, Developmental Studies Hybridoma Bank, The University of Iowa, Iowa City, IA), monoclonal anti-neuronal tubulin β III antibody (TuJ1; Covance), polyclonal anti-UCH-L1 antibody (PGP9.5; RA95101, UltraClone), and polyclonal anti-FLAG antibody (Sigma). All secondary polyclonal antibodies conjugated to Alexa Fluor fluorescein were purchased from Molecular Probes.

### Cortical NPC culture and differentiation conditions in C57BL/6 mice

Cortical NPCs were cultured as previously described (Nakashima et al., 1999). Briefly, embryos were removed from pregnant C57BL/6J mice (CLEA Japan) and staged according to morphological criteria to confirm the gestational day (Kaufman et al., 1998). Developing mouse cerebral cortex was dissected from E14 embryos. Cells were mechanically dissociated by trituration and plated at a concentration of $3.0\times10^6$ cells per 10 cm dish (Becton Dickinson) precoated with 10 ml of 15 μg/ml poly-L-ornithine (Sigma) and 10 ml of 1 μg/ml fibronectin (Nitta Gelatin). Cells were expanded for 5 days in serum-free neurobasal (NB) medium (Invitrogen) supplemented with B27 (Invitrogen), 0.5 mM L-glutamine (Invitrogen), 100 U/ml penicillin and 100 μg/ml streptomycin (Invitrogen). This medium contained 10 ng/ml bFGF (PeproTech). Cultures were maintained at 37°C in an atmosphere of 95% air and 5% $CO_2$. For secondary culture, bFGF-expanded NPCs were washed in warm Hank's Balanced Salt Solution, detached with mechanical pipetting, and resuspended in NB medium supplemented with B27, but not bFGF. Cells were then replated in 24-well plates (Nunc; $1.8\times10^5$ cells per well) that were precoated with 500 μl of 15 μg/ml poly-L-ornithine and 500 μl of 1 μg/ml fibronectin for immunofluorescence staining at each time point.

### Cortical NPC culture and differentiation conditions in *gad* mice

Culture of NPCs derived from *gad* mice was performed as with NPCs derived from B6 mice. Developing mouse cerebral cortex was dissected from embryos at E13.5 to E14.5. The precise gestational day was determined according to previously established morphological criteria (Kaufman et al., 1998). NPCs from each embryo were collected and cultured separately. Each genotype was determined later using PCR and, as a result, each pair of *gad* and control littermate mice from two sets of

parents were used. Each culture of NPCs was replated in 24-well plates without bFGF and stained using anti-UCH-L1 24 hours after plating.

### Immunohistochemistry

Brain sections were stained as previously described (Li et al., 2003; Osaka et al., 2003). Briefly, E14 and E16 mouse brains were removed and fixed in 4% paraformaldehyde/phosphate-buffered saline (PBS) for 2 hours at room temperature, cryoprotected in 30% sucrose in PBS and frozen in dry ice. Sections (20 μm thick) were cut on a cryostat, and mounted on aminopropylsilane (APS)-coated glass slides. They were then washed three times in PBS for 5 minutes, and blocked for 1 hour at room temperature with 3% bovine serum albumin, 2% (v/v) normal goat serum, and 0.2% (v/v) Triton X-100 in PBS (pH 7.4). Sections were incubated with primary antibodies [anti-nestin antibody (Rat401) 1:10; or anti-UCH-L1 antibody (RA95101) 1:4000; or anti-TuJ1 antibody, 1:1000] overnight at 4°C or for 2 hours at room temperature. After rinsing in PBS, the sections were incubated for 2 hours with diluted fluorescein-conjugated secondary antibody (1:200). The images were obtained with a confocal laser scanning TCS SL microscope, and detailed analyses were performed using an LSC confocal microscope system (Leica). Immunofluorescence intensities were measured from confocal images with Mac SCOPE software (version 2.59; Mitani).

### Immunocytochemistry

Cells were stained as previously described (Aoki et al., 2002). Briefly, all incubations and washes were performed at room temperature. Cells were fixed with 3.8% formaldehyde/PBS for 10 minutes and permeabilized with 0.02% (v/v) Triton X-100/PBS for 5 minutes. Fixed cells were blocked with 3.3% goat serum for 30 minutes. Cells were incubated with a diluted primary polyclonal or monoclonal antibody (both were used for double staining) for 0.5-1 hour. The cells were then incubated with diluted secondary antibody conjugated to fluorescein for 0.5-1 hour. Antibody dilutions were as follows: anti-UCH-L1 antibody, 1:4000; anti-nestin antibody, 1:500; anti-TuJ1, 1:500. All secondary antibodies were diluted 1:200 in 1% goat serum/PBS before use. The images were obtained with fluorescence microscopy on an IX70 microscope (Olympus).

### Transfection

For C57BL/6 mice, cells replated in 24-well plates were cultured overnight in growth medium containing bFGF and B27. The next day, each construct was transfected using Lipofectamine 2000 (Invitrogen) according to the manufacturer's instructions. NPCs were allowed to proliferate for 48 hours after transfection and then induced to differentiate for 12 hours without bFGF. For *gad*-mouse-derived NPCs, transfection was done in a similar manner.

### Expression plasmids for human UCH-L1 variants

Mutant cDNAs encoding human UCH-L1 containing either the D30A or C90S substitution were obtained using the QuikChange site-directed mutagenesis kit (Stratagene) with the following mutagenesis oligonucleotides: 5′-CAGTGG-CGCTTCGTGGCCGTGCTGGGGCTGGAAG-3′ and 5′-CTTCCAGCCCCAG-CACGGCCACGAAGCGCCACTG-3′ for D30A; 5′-CCATTGGGAATTCCTCT-GGCACAATCGGAC-3′ and 5′-GTCCGATTGTGCCACAGGAATTCCCAA-TGG-3′ for C90S. Each single-nucleotide mutation in the resulting plasmids was confirmed by sequencing. Mammalian expression plasmids containing either FLAG-tagged human WT UCH-L1 or the D30A or C90S mutants were constructed using a pCI-*neo* mammalian expression vector (Promega). Bacterial expression plasmids containing either 6HN-tagged human WT UCH-L1 or the D30A or C90S mutants were constructed using a tetracycline-inducible expression system. *Xho*I-*Not*I cDNA fragments of the pCI-*neo* WT UCH-L1 or the D30A and C90S mutants and constructs were digested, and the DNA fragments were ligated between the *Sal*I and *Not*I sites in pPROtetE233 (Clontech) to generate pPROtetE233 6HN-tagged human WT, D30A and C90S UCH-L1 vectors. These expression plasmids were confirmed by sequencing.

### In vitro assay for human UCH-L1 activity

Purified human UCH-L1 and the fluorogenic substrate ubiquitin-7-amino-4-methylcoumarin (Ub-AMC; Boston Biochem) were used to determine steady-state kinetic parameters as described previously (Nishikawa et al., 2003).

### Immunoprecipitation

NIH-3T3 cells stably expressing human WT UCH-L1 or the C90S or D30A mutants, all with an HA-FLAG double tag at the N terminus, were cultured to subconfluency in a 10 cm dish, lyzed with 1 ml of modified RIPA buffer [50 mM Tris-HCl, pH 7.5, 1% (v/v) NP-40, 0.25% sodium deoxycholate, 150 mM NaCl, 1 mM EDTA] with EDTA-free complete protease inhibitor cocktail (Roche), sonicated and centrifuged at 18,000 *g* for 20 minutes at 4°C. Immunoprecipitation was performed as described previously (Ogawa et al., 2002).

### Statistics

Statistical analyses were performed using StatView, version 5.0 (SAS) and Prism, version 3 (GraphPad Software). Analysis of variance (ANOVA) was used to assess differences between groups. A $P$ value of less than 0.05 was considered statistically significant. When ANOVA results were statistically significant, they were examined by Fisher's PLSD, or Dunnett's multiple comparison test, or Bonferroni-Dunn multiple comparisons post hoc test. Differences between *gad* mice and control mice were analyzed using the Mann-Whitney U test.

The authors thank Yuh Nung Jan and Hua-Shun Li for providing the immunohistochemistry methods; Yoshihiro Nakatani and Hidesato Ogawa for providing the retroviral expression system and immunoprecipitation methods; and Masako Shikama for the care and breeding of animals. This work was supported by Grants-in-Aid for Scientific Research from the Ministry of Health, Labour and Welfare of Japan, and Grants-in-Aid for Scientific Research from the Ministry of Education, Culture, Sports, Science and Technology of Japan.

## References

**Aoki, S., Su, Q., Li, H., Nishikawa, K., Ayukawa, K., Hara, Y., Namikawa, K., Kiryu-Seo, S., Kiyama, H. and Wada, K.** (2002). Identification of an axotomy-induced glycosylated protein, AIGP1, possibly involved in cell death triggered by endoplasmic reticulum-Golgi stress. *J. Neurosci.* **22**, 10751-10760.

**Arnaud, L., Ballif, B. A. and Cooper, J. A.** (2003). Regulation of protein tyrosine kinase signaling by substrate degradation during brain development. *Mol. Cell. Biol.* **23**, 9293-9302.

**Bock, H. H., Jossin, Y., May, P., Bergner, O. and Herz, J.** (2004). Apolipoprotein E receptors are required for reelin-induced proteasomal degradation of the neuronal adaptor protein Disabled-1. *J. Biol. Chem.* **279**, 33471-33479.

**Dickson, D. W., Schmidt, M. L., Lee, V. M., Zhao, M. L., Yen, S. H. and Trojanowski, J. Q.** (1994). Immunoreactivity profile of hippocampal CA2/3 neurites in diffuse Lewy body disease. *Acta Neuropathol. (Berl.)* **87**, 269-276.

**Fukuda, S., Kato, F., Tozuka, Y., Yamaguchi, M., Miyamoto, Y. and Hisatsune, T.** (2003). Two distinct subpopulations of nestin-positive cells in adult mouse dentate gyrus. *J. Neurosci.* **23**, 9357-9366.

**Hartfuss, E., Forster, E., Bock, H. H., Hack, M. A., Leprince, P., Luque, J. M., Herz, J., Frotscher, M. and Gotz, M.** (2003). Reelin signaling directly affects radial glia morphology and biochemical maturation. *Development* **130**, 4597-4609.

**Hashimoto, M. and Mikoshiba, K.** (2004). Neuronal birthdate-specific gene transfer with adenoviral vectors. *J. Neurosci.* **24**, 286-296.

**Kaufman, M. H., Brune, R. M., Davidson, D. R. and Baldock, R. A.** (1998). Computer-generated three-dimensional reconstructions of serially sectioned mouse embryos. *J. Anat.* **193**, 323-336.

**Kawauchi, T., Chihama, K., Nabeshima, Y. and Hoshino, M.** (2003). The in vivo roles of STEF/Tiam1, Rac1 and JNK in cortical neuronal migration. *EMBO J.* **22**, 4190-4201.

**Kwon, J., Kikuchi, T., Setsuie, R., Ishii, Y., Kyuwa, S. and Yoshikawa, Y.** (2003). Characterization of the testis in congenitally ubiquitin carboxy-terminal hydrolase-1 (Uch-L1) defective (gad) mice. *Exp. Anim.* **52**, 1-9.

**Larsen, C. N., Krantz, B. A. and Wilkinson, K. D.** (1998). Substrate specificity of deubiquitinating enzymes: ubiquitin C-terminal hydrolases. *Biochemistry* **37**, 3358-3368.

**Leroy, E., Boyer, R., Auburger, G., Leube, B., Ulm, G., Mezey, E., Harta, G., Brownstein, M. J., Jonnalagada, S., Chernova, T. et al.** (1998). The ubiquitin pathway in Parkinson's disease. *Nature* **395**, 451-452.

**Li, H. S., Wang, D., Shen, Q., Schonemann, M. D., Gorski, J. A., Jones, K. R., Temple, S., Jan, L. Y. and Jan, Y. N.** (2003). Inactivation of Numb and Numblike in embryonic dorsal forebrain impairs neurogenesis and disrupts cortical morphogenesis. *Neuron* **40**, 1105-1118.

**Liu, Y., Fallon, L., Lashuel, H. A., Liu, Z. and Lansbury, P. T., Jr** (2002). The UCH-L1 gene encodes two opposing enzymatic activities that affect alpha-synuclein degradation and Parkinson's disease susceptibility. *Cell* **111**, 209-218.

**Liu, Y., Lashuel, H. A., Choi, S., Xing, X., Case, A., Ni, J., Yeh, L. A., Cuny, G. D., Stein, R. L. and Lansbury, P. T., Jr** (2003). Discovery of inhibitors that elucidate the role of UCH-L1 activity in the H1299 lung cancer cell line. *Chem. Biol.* **10**, 837-846.

**Malatesta, P., Hartfuss, E. and Gotz, M.** (2000). Isolation of radial glial cells by fluorescent-activated cell sorting reveals a neuronal lineage. *Development* **127**, 5253-5263.

**Malatesta, P., Hack, M. A., Hartfuss, E., Kettenmann, H., Klinkert, W., Kirchhoff, F. and Gotz, M.** (2003). Neuronal or glial progeny: regional differences in radial glia fate. *Neuron* **37**, 751-764.

**McQuaid, S., McConnell, R., McMahon, J. and Herron, B.** (1995). Microwave antigen retrieval for immunocytochemistry on formalin-fixed, paraffin-embedded post-mortem CNS tissue. *J. Pathol.* **176**, 207-216.

**Nadarajah, B., Brunstrom, J. E., Grutzendler, J., Wong, R. O. and Pearlman, A. L.** (2001). Two modes of radial migration in early development of the cerebral cortex. *Nat. Neurosci.* **4**, 143-150.

**Nakashima, K., Yanagisawa, M., Arakawa, H., Kimura, N., Hisatsune, T., Kawabata, M., Miyazono, K. and Taga, T.** (1999). Synergistic signaling in fetal brain by STAT3-Smad1 complex bridged by p300. *Science* **284**, 479-482.

**Nishikawa, K., Li, H., Kawamura, R., Osaka, H., Wang, Y. L., Hara, Y., Hirokawa, T., Manago, Y., Amano, T., Noda, M. et al.** (2003). Alterations of structure and

hydrolase activity of parkinsonism-associated human ubiquitin carboxyl-terminal hydrolase L1 variants. *Biochem. Biophys. Res. Commun.* **304**, 176-183.

**Noctor, S. C., Flint, A. C., Weissman, T. A., Dammerman, R. S. and Kriegstein, A. R.** (2001). Neurons derived from radial glial cells establish radial units in neocortex. *Nature* **409**, 714-720.

**Noctor, S. C., Flint, A. C., Weissman, T. A., Wong, W. S., Clinton, B. K. and Kriegstein, A. R.** (2002). Dividing precursor cells of the embryonic cortical ventricular zone have morphological and molecular characteristics of radial glia. *J. Neurosci.* **22**, 3161-3173.

**Noctor, S. C., Martinez-Cerdeno, V., Ivic, L. and Kriegstein, A. R.** (2004). Cortical neurons arise in symmetric and asymmetric division zones and migrate through specific phases. *Nat. Neurosci.* **7**, 136-144.

**Ogawa, H., Ishiguro, K., Gaubatz, S., Livingston, D. M. and Nakatani, Y.** (2002). A complex with chromatin modifiers that occupies E2F- and Myc-responsive genes in G0 cells. *Science* **296**, 1132-1136.

**Osaka, H., Wang, Y. L., Takada, K., Takizawa, S., Setsuie, R., Li, H., Sato, Y., Nishikawa, K., Sun, Y. J., Sakurai, M. et al.** (2003). Ubiquitin carboxy-terminal hydrolase L1 binds to and stabilizes monoubiquitin in neuron. *Hum. Mol. Genet.* **12**, 1945-1958.

**Patrick, G. N., Zhou, P., Kwon, Y. T., Howley, P. M. and Tsai, L. H.** (1998). p35, the neuronal-specific activator of cyclin-dependent kinase 5 (Cdk5) is degraded by the ubiquitin-proteasome pathway. *J. Biol. Chem.* **273**, 24057-24064.

**Qian, X., Goderie, S. K., Shen, Q., Stern, J. H. and Temple, S.** (1998). Intrinsic programs of patterned cell lineages in isolated vertebrate CNS ventricular zone cells. *Development* **125**, 3143-3152.

**Qian, X., Shen, Q., Goderie, S. K., He, W., Capela, A., Davis, A. A. and Temple, S.** (2000). Timing of CNS cell generation: a programmed sequence of neuron and glial cell production from isolated murine cortical stem cells. *Neuron* **28**, 69-80.

**Qiu, L., Joazeiro, C., Fang, N., Wang, H. Y., Elly, C., Altman, Y., Fang, D., Hunter, T. and Liu, Y. C.** (2000). Recognition and ubiquitination of Notch by Itch, a hect-type E3 ubiquitin ligase. *J. Biol. Chem.* **275**, 35734-35737.

**Rice, D. S. and Curran, T.** (2001). Role of the reelin signaling pathway in central nervous system development. *Annu. Rev. Neurosci.* **24**, 1005-1039.

**Roegiers, F. and Jan, Y. N.** (2004). Asymmetric cell division. *Curr. Opin. Cell Biol.* **16**, 195-205.

**Saigoh, K., Wang, Y. L., Suh, J. G., Yamanishi, T., Sakai, Y., Kiyosawa, H., Harada, T., Ichihara, N., Wakana, S., Kikuchi, T. et al.** (1999). Intragenic deletion in the gene encoding ubiquitin carboxy-terminal hydrolase in gad mice. *Nat. Genet.* **23**, 47-51.

**Satoh, J. and Kuroda, Y.** (2001). A polymorphic variation of serine to tyrosine at codon 18 in the ubiquitin C-terminal hydrolase-L1 gene is associated with a reduced risk of sporadic Parkinson's disease in a Japanese population. *J. Neurol. Sci.* **189**, 113-117.

**Sauvageot, C. M. and Stiles, C. D.** (2002). Molecular mechanisms controlling cortical gliogenesis. *Curr. Opin. Neurobiol.* **12**, 244-249.

**Schofield, J. N., Day, I. N., Thompson, R. J. and Edwards, Y. H.** (1995). PGP9.5, a ubiquitin C-terminal hydrolase; pattern of mRNA and protein expression during neural development in the mouse. *Brain Res. Dev. Brain Res.* **85**, 229-238.

**Sekiguchi, S., Yoshikawa, Y., Tanaka, S., Kwon, J., Ishii, Y., Kyuwa, S., Wada, K., Nakamura, S. and Takahashi, K.** (2003). Immunohistochemical analysis of protein gene product 9.5, a ubiquitin carboxyl-terminal hydrolase, during placental and embryonic development in the mouse. *Exp. Anim.* **52**, 365-369.

**Shen, Q., Qian, X., Capela, A. and Temple, S.** (1998). Stem cells in the embryonic cerebral cortex: their role in histogenesis and patterning. *J. Neurobiol.* **36**, 162-174.

**Sullivan, M. L. and Vierstra, R. D.** (1993). Formation of a stable adduct between ubiquitin and the Arabidopsis ubiquitin-conjugating enzyme, AtUBC1+. *J. Biol. Chem.* **268**, 8777-8780.

**Tabata, H. and Nakajima, K.** (2003). Multipolar migration: the third mode of radial neuronal migration in the developing cerebral cortex. *J. Neurosci.* **23**, 9996-10001.

**Temple, S.** (2001). The development of neural stem cells. *Nature* **414**, 112-117.

**Weissman, A. M.** (2001). Themes and variations on ubiquitylation. *Nat. Rev. Mol. Cell. Biol.* **2**, 169-178.

**Wilkinson, K. D., Lee, K. M., Deshpande, S., Duerksen-Hughes, P., Boss, J. M. and Pohl, J.** (1989). The neuron-specific protein PGP 9.5 is a ubiquitin carboxyl-terminal hydrolase. *Science* **246**, 670-673.

**Zhong, W., Feder, J. N., Jiang, M. M., Jan, L. Y. and Jan, Y. N.** (1996). Asymmetric localization of a mammalian numb homolog during mouse cortical neurogenesis. *Neuron* **17**, 43-53.

**Zhong, W., Jiang, M. M., Weinmaster, G., Jan, L. Y. and Jan, Y. N.** (1997). Differential expression of mammalian Numb, Numblike and Notch1 suggests distinct roles during mouse cortical neurogenesis. *Development* **124**, 1887-1897.

Journal of Cell Science